Hydrogenolysis of Ethane, Propane, *n*-Butane, and Neopentane on the (111) and (110)-(1×2) Surfaces of Iridium

J. R. Engstrom,[†,‡] D. W. Goodman,*[,‡] and W. H. Weinberg*[,§]

Contribution from the Surface Science Division, Sandia National Laboratories, Albuquerque, New Mexico 87185, and Division of Chemistry and Chemical Engineering, California Institute of Technology, Pasadena, California 91125. *Received February 1, 1988*

Abstract: The hydrogenolysis of ethane, propane, *n*-butane, and neopentane has been investigated on the (111) and (110)-(1×2) single-crystalline surfaces of iridium at reactant partial pressures between 0.2 and 5.0 Torr of hydrocarbon and between 20 and 500 Torr of hydrogen and for surface temperatures from 400 to 700 K. A coupled high-pressure reactor–ultrahigh vacuum analysis chamber was employed, which permitted both the measurement of the specific rates of reaction and in situ pre- and postreaction surface characterization. Both the apparent reaction kinetics (activation energies and preexponential factors) and the dependence of the rates of reaction on the reactant partial pressures (apparent reaction "orders") were examined in detail. Postreaction surface analysis by Auger electron spectroscopy indicated the presence of a *submonolayer* carbonaceous residue, the coverage of which was nearly identical on both surfaces and essentially independent of reaction conditions, i.e. surface temperature and reactant partial pressures. Titration of these residues with hydrogen produced only methane in all cases, suggesting that the carbonaceous residue plays the role of a "spectator". The major reaction channel for ethane, propane, and neopentane involves the cleavage of a single carbon–carbon bond, resulting in "demethylization" of the parent hydrocarbon. For *n*-butane, the major reaction channels on the two surfaces are $n\text{-}C_4H_{10} + 2H_2 \rightarrow 2CH_4 + C_2H_6$ on Ir(111) and $n\text{-}C_4H_{10} + H_2 \rightarrow 2C_2H_6$ on Ir(110)-(1×2). In all cases, at sufficiently high temperatures, the apparent activation energy decreases and the selectivity for methane increases greatly. These changes have been identified with a depletion in the steady-state coverage of hydrogen adatoms as the temperature is increased. A mechanistic model involving a rate-limiting, irreversible, "unimolecular" C–C bond cleavage step has been employed to describe the variations in the specific activity and selectivity of hydrogenolysis with variations in both the temperature and the reactant partial pressures. The apparent kinetic parameters implicated by this model, which represent combinations of rate coefficients of several elementary reactions, have been found to be consistent with the expected values for the preexponential factors of the contributing elementary reactions. In addition, the application of this model to the data [with the exception of *n*-butane on Ir(110)-(1×2)] permitted a determination of the stoichiometries of the adsorbed parent hydrocarbon fragments (i.e. reaction intermediates). In all cases, the implied stoichiometries are consistent with the proposition that hydrogenolysis proceeds through a partially dehydrogenated intermediate that is multiply bound to the surface via one or more surface metal atoms. The hydrogenolysis of *n*-butane on the Ir(110)-(1×2) surface is not described well by the mechanism involving irreversible C–C bond cleavage; rather, a mechanism involving reversible C–C bond cleavage in the adsorbed reaction intermediate describes the data best. The hydrogenolysis of ethane proceeds through different reaction intermediates, the parent fragment on the Ir(110)-(1×2) surface being more extensively dehydrogenated. The observation of a relatively larger apparent preexponential factor for the reaction of ethane on the Ir(110)-(1×2) surface has been found to be consistent with a more extensively dehydrogenated intermediate. The apparent kinetic parameters and the implicated reaction intermediates (i.e. mechanisms) for both propane and neopentane are nearly indistinguishable on the two surfaces. The selectivity for the hydrogenolysis of *n*-butane on the two surfaces is due to the occurrence of different adsorbed reaction intermediates. It is suggested that the intermediate that leads to the high selectivity for ethane on the Ir(110)-(1×2) surface is a mononuclear metallacycle pentane, the formation of which is sterically forbidden on the (111) surface. The implication of this proposition (i.e. different mechanisms for *n*-butane hydrogenolysis) for related reactions of saturated hydrocarbons, such as skeletal isomerization and cyclization, is discussed briefly.

I. Introduction

Study of the reactions of saturated hydrocarbons with hydrogen on transition-metal surfaces is of considerable technological importance, most notably in connection with the hydroprocessing of petrochemical feedstocks. The hydrogenolysis of saturated hydrocarbons represents a major subset of the reactions that occur on supported transition-metal catalysts, which also include, for example, skeletal isomerization and cyclization. For many of these reactions the *specific* activity (per site basis) and the selectivity have been found to be sensitive to the average metallic particle size. This "structure-sensitivity"[1] has been attributed to a number of effects, which include variations in the electronic and/or geometric nature of the catalyst surface with particle size. Although considerable work has been carried out in this area,[2-7] a *microscopic* understanding of the observed variations in the catalytic properties with particle size has not been forthcoming. For example, few correlations exist between the structure of the catalyst surface and the relevant adsorbed reaction intermediates that act to control the activity and/or selectivity of a particular catalyst.

We have undertaken a fundamental examination of the role of surface structure in the hydrogenolysis of various short-chain alkanes on two oriented single-crystalline surfaces of iridium. The use of oriented single crystals as catalysts allows an *unambiguous* assessment of the effects of surface geometry[8] or, equivalently, surface electronic structure as a consequence of its geometry. For example, previous work[9-11] has indicated that the specific rates of hydrogenolysis of various alkanes differ considerably on two different high-symmetry single-crystalline surfaces of nickel, namely the Ni(100) and Ni(111) planes. It is important to note

[†] Visiting from the Division of Chemistry and Chemical Engineering, California Institute of Technology, Pasadena, CA 91125. Present address: Department of Chemistry, University of Washington, Seattle, WA 98195.
[‡] Sandia National Laboratories.
[§] California Institute of Technology.

(1) Boudart, M. *Adv. Catal.* **1969**, *20*, 153.
(2) Sinfelt, J. H. *Catal. Rev.* **1969**, *3*, 175; *Adv. Catal.* **1973**, *23*, 91.
(3) Anderson, J. R. *Adv. Catal.* **1973**, *23*, 1.
(4) Clarke, J. K. A.; Rooney, J. J. *Adv. Catal.* **1976**, *25*, 125.
(5) Gault, F. G. *Adv. Catal.* **1981**, *30*, 1.
(6) Paal, Z.; Tetenyi, P. In *Catalysis (Specialist Periodical Reports)*; Bond, G. C., Webb, G., Eds.; Royal Society of Chemistry: London, 1982; Vol. 5, p 80.
(7) Maire, G. L. C.; Garin, F. G. In *Catalysis—Science and Technology*; Anderson, J. R., Boudart, M., Eds.; Springer-Verlag: Berlin, 1984; Vol. 6, p 161.
(8) Goodman, D. W.; Kelley, R. D.; Madey, T. E.; Yates, J. T., Jr. *J. Catal.* **1980**, *63*, 226; Goodman, D. W. *Acc. Chem. Res.* **1984**, *17*, 194.
(9) Goodman, D. W. *Surf. Sci.* **1982**, *123*, L679.
(10) Goodman, D. W. *Proc. Int. Congr. Catal. 8th* **1984**, *4*, 3.
(11) Goodman, D. W. *J. Vac. Sci. Technol., A* **1984**, *2*, 873.

0002-7863/88/1510-8305$01.50/0

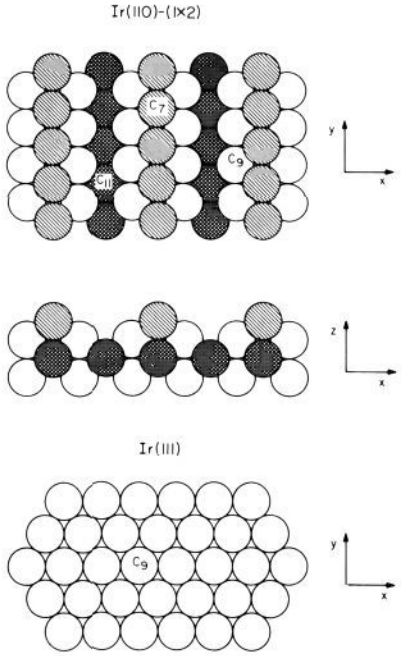

Figure 1. Structural models for the (110)-(1×2) and (111) surfaces of iridium. The z-axis is perpendicular to the plane of the surface. The C_n designate the coordination numbers of the metal surface atoms.[13]

that, for idealized catalyst particle shapes (e.g. cubooctahedra), the relative number of atoms in these two high-symmetry microfacets will vary with particle size. One also expects a variation in the relative number of atoms in the low coordination number edge and corner positions where these high-symmetry planes intersect. In order to determine the importance of the latter, we have employed the close-packed (111) and the corrugated (110)-(1×2) surfaces of iridium as model catalysts. The clean Ir(110) surface reconstructs into a (1×2) superstructure,[12] which contains a large fraction (25%) of low coordination number [C_7[13]] edge atoms, whereas a perfect (111) surface contains no such atoms (cf. Figure 1). The (1×2) reconstruction is expected to be stable under reaction conditions, i.e. in the presence of adsorbed hydrocarbon residues and/or surface carbon and hydrogen.[14] Thus, if the ratio of the number of edge atoms to the number of face atoms influences the kinetics and/or mechanism of a particular reaction, then the (110)-(1×2) and (111) surfaces should be decisive in quantifying the connection between catalytic activity and/or selectivity and *local* surface structure.

We shall consider here the reactions of ethane, propane, *n*-butane, and neopentane with hydrogen on these two single-crystalline surfaces of iridium. When the reactions of these four hydrocarbons of differing structure are examined, various adsorption mechanisms can be isolated and their relative contributions can be evaluated, e.g. "1,2" adsorption is prohibited for neopentane, whereas "1,4" adsorption is possible only for *n*-butane. Since the heat- and mass-transfer limitations associated with single-crystalline catalysts are not as restrictive as those for supported metal catalysts, the reaction conditions (i.e. reactant partial pressures and surface temperature) can be varied over a wide range. These data can be utilized to evaluate the apparent kinetics of the reaction and the selectivity as a function of surface temperature. Moreover, by varying the reactant partial pressures, the importance of proposed reaction mechanisms can be assessed, and, in principle, the stoichiometry of the relevant adsorbed intermediates can be deduced.[15,16] Of crucial importance, especially in connection with reactions of hydrocarbons, is the availability of postreaction surface analysis. This permits a decoupling of changes in the activity and selectivity with reaction conditions that are *intrinsic*, as opposed to those that are due, for example, to a variation in the coverage of a carbonaceous residue. Finally, by comparison of the results obtained on both surfaces, insight can be obtained concerning the role of surface structure in dictating the particular adsorbed intermediates in each case and, hence, the catalytic selectivity.

Table I. Carbonaceous Residue Following Hydrogenolysis Reactions on the Ir(111) Surface

reactant	fractional carbon coverage, θ_C
ethane	0.17 ± 0.04
propane	0.28 ± 0.10
n-butane	0.34 ± 0.08
neopentane	0.45 ± 0.10

II. Experimental Procedures

The experiments described here were performed in a high-pressure reaction chamber (total volume ≃600 cm^3) linked to an ultrahigh vacuum (UHV) analysis chamber, similar to that described previously.[8] The chambers, which are pumped separately, are connected by a metal valve, and the base pressure in both is 10^{-10} Torr. In the UHV analysis chamber, facilities are available for Auger electron spectroscopy, ion sputtering, and mass spectrometry. The catalyst samples are attached to a retraction bellows and can be translated vertically to various positions in either chamber. The single-crystal catalysts of iridium (total surface area ≃1 cm^2) were mounted on tungsten leads and were heated resistively. The temperature was controlled manually and was measured with a W/5% Re–W/26% Re thermocouple spotwelded to the crystal. A consideration of both the mean free paths of the gas-phase reactants, corresponding to the pressures examined here (20–500 Torr), and the relative geometry of the reaction chamber [e.g. the surface area of the crystal and the distance between the crystal and the (room-temperature) chamber walls] indicates that the gas and surface temperatures are essentially equivalent. The crystals were cleaned in the UHV analysis chamber by argon ion sputtering, heating in 5×10^{-7} Torr of oxygen at 700 K, and annealing to 1600 K. Surface cleanliness was verified by Auger electron spectroscopy.

The ethane (99.99%), propane (99.97%), and *n*-butane (99.9%) employed in these experiments were research purity from Matheson. The neopentane was ultrahigh purity (99.995%) from API Standard Reference Materials, and the hydrogen was also ultrahigh purity (99.999%).[17] The hydrocarbons were purified further by degassing at 80 K, followed by triple distillation from a liquid pentane/solid pentane bath. Reaction products were detected by gas chromatography, which, in this case, is superior to mass spectrometry (e.g. there are no complications due to the interpretation of fragmentation patterns). Absolute reaction rates were calculated by utilizing the measured volume of the reactor, the reaction time (i.e. batch reactor kinetics), and the measured geometrical surface areas of the crystals. Specific rates were calculated by using substrate densities of 1.57×10^{15} and 1.93×10^{15} sites·cm^{-2} for the (111) and (110)-(1×2) surfaces, respectively. The corresponding saturation coverages of hydrogen (in these cases, the coverage that is irreversibly adsorbed at 100 K), commonly used to determine metallic surface areas of supported catalysts, are within approximately 20% of these substrate densities in each case.[19] It should be noted, however, that if the low coordination number (C_7) surface atoms provide the "active sites" for a particular reaction (cf. Figure 1), then this procedure will *underestimate* the specific rate for the Ir(110)-(1×2) surface by a factor of 4.

III. Results

A. Ir(111) Surface. Specific rates of hydrogenolysis of ethane, propane, *n*-butane, and neopentane on the Ir(111) surface are

(12) Chan, C.-M.; Van Hove, M. A.; Weinberg, W. H.; Williams, E. D. *Solid State Commun.* **1979**, *30*, 47. Chan, C.-M.; Van Hove, M. A.; Weinberg, W. H.; Williams, E. D. *Surf. Sci.* **1980**, *91*, 430.

(13) van Hardeveld, R.; Hartog, F. *Adv. Catal.* **1972**, *22*, 75.

(14) Under nonreactive conditions, the presence of hydrocarbon fragments, carbon and/or hydrogen does not lift the (1×2) surface reconstruction; see, for example: Weinberg, W. H. *Surv. Prog. Chem.* **1983**, *10*, 1.

(15) Cimino, A.; Boudart, M.; Taylor, H. S. *J. Phys. Chem.* **1954**, *58*, 796.

(16) Sinfelt, J. H. *J. Catal.* **1972**, *27*, 468.

(17) Ultrahigh-purity reactants are desirable in order to reduce any extraneous contamination of the catalyst surface. For example, olefins, if present in sufficient concentrations, can lead to an increased concentration of adsorbed carbonaceous residue.[18]

(18) Engstrom, J. R.; Goodman, D. W.; Weinberg, W. H., to be submitted for publication.

(19) Engstrom, J. R.; Tsai, W.; Weinberg, W. H. *J. Chem. Phys.* **1987**, *87*, 3104. Ibbotson, D. E.; Wittrig, T. S.; Weinberg, W. H. *J. Chem. Phys.* **1980**, *72*, 4885.

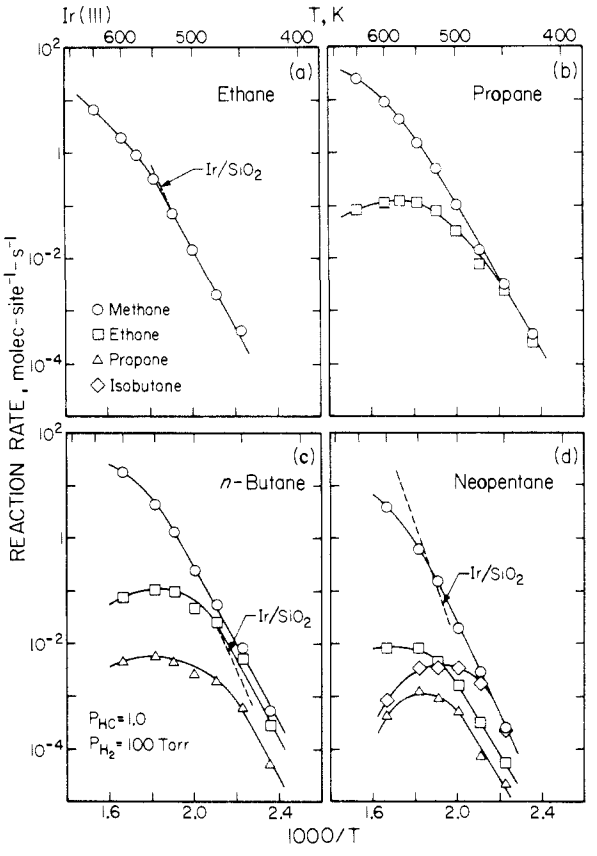

Figure 2. Specific reaction rates (product molecules·site^{-1}·s^{-1}) for the hydrogenolysis of (a) ethane, (b) propane, (c) *n*-butane, and (d) neopentane on the Ir(111) surface. The partial pressure of hydrocarbon was 1.0 Torr, whereas that of hydrogen was 100 Torr. The dashed lines in (a), (c), and (d) represent data obtained by Foger and Anderson[22] on a 0.98 wt % Ir/SiO_2 catalyst ($\bar{d}_{Ir}$ = 70 Å, dispersion of 16%) extrapolated to our reactant partial pressures and plotted in terms of conversion.

shown in parts a–d of Figure 2, plotted in Arrhenius form. These data represent *steady-state* reaction rates, as verified by measuring the total amount of product formed after various times of reaction, typically 50–2000 s, depending on the temperature. No induction periods were detected. To avoid secondary reactions, conversions were restricted typically to below 1%. The "standard" reactant partial pressure ratio, H_2/C_nH_{2n+2}, was 100/1, with a hydrocarbon pressure of 1.0 Torr.

Postreaction surface characterization by Auger electron spectroscopy indicated the presence of a *submonolayer* carbonaceous residue, the fractional coverage of which was essentially independent of reaction conditions in all cases [surface temperature *and* reactant partial pressures (see below)]. The measured values for the coverages are given in Table I in terms of a fractional carbon coverage, where $\theta_c = 1$ is equivalent to the substrate density, in this case 1.57×10^{15} atoms·cm^{-2}. There is an approximately linear increase in the carbon coverage with increasing size of the parent hydrocarbon (i.e. the coverage of the carbonaceous residue with respect to the parent admolecule has the nearly constant value of 0.1 site^{-1}). Postreaction thermal desorption from the surface containing the carbonaceous residue produced only H_2, which gave a broad desorption feature in all cases, evolving H_2 between approximately 350 and 800 K, and exhibiting a peak temperature of approximately 500 K. No attempts were made to determine the average stoichiometry (C_xH_y) of this carbonaceous residue since, as we shall demonstrate, it is not representative of the relevant adsorbed reaction intermediates under reaction conditions. The unimportance of the carbonaceous residue in regard to the major reaction channels was demonstrated by returning the catalyst to the reaction chamber (i.e. after the reactants had been pumped away) and titrating the carbonaceous residue with pure hydrogen (100 Torr) at the relevant reaction temperature. Methane was the *only* product observed in all cases; no "C_{n-1}" products were produced. For example, the relative selectivity, CH_4/C_2H_6, for propane hydrogenolysis has been found to be equal to 1.8 at T = 475 (cf. Figure 2). However, titration of the carbonaceous residue with 100 Torr of H_2 at 475 K produced only methane. In addition, the corresponding rate of methane production from the titration procedure was at least a factor of 10 smaller than that measured in the presence of 1 Torr of propane. Thus, due to both the absence of ethane production and the much smaller rate of methane production from the titration procedure, we conclude that the reaction channel involving the carbonaceous residue makes only a minor contribution to the measured rates of hydrogenolysis reported here.[20]

As may be seen in Figure 2, the only reaction products observed were methane, ethane, propane, and isobutane. With the exception of *n*-butane, the major reaction channels at sufficiently low temperatures ($T \leq 475$ K) are given by

$$C_nH_{2n+2} + H_2 \rightarrow CH_4 + C_{n-1}H_{2(n-1)+2}$$

i.e. the products expected from the cleavage of a single carbon–carbon bond. For *n*-butane, the major reaction channel is given by

$$n\text{-}C_4H_{10} + 2H_2 \rightarrow 2CH_4 + C_2H_6$$

i.e. two carbon–carbon bonds are cleaved.

No isomerization products were detected from either *n*-butane (i.e. isobutane) or neopentane (i.e. isopentane or *n*-pentane). For the case of *n*-butane, on the basis of the sensitivity of our gas chromatographic detection, the maximum rate of production of isobutane is below 10^{-4} molecules·site^{-1}·s^{-1} for all reaction conditions considered. This observation is consistent with the fact that, to the best of our knowledge, the isomerization of *n*-butane to isobutane has not been reported on iridium catalysts. A similar analysis for neopentane was hampered by the fact that the isomerization products are located on the trailing edge of the (considerably larger) parent hydrocarbon chromatographic peak. A conservative estimate, however, places the maximum rate of isomerization below that of the total rate of hydrogenolysis, a result that is consistent with previous work. For example, both Boudart and Ptak[21] and Foger and Anderson[22] have reported an isomerization rate (to isopentane) on silica-supported iridium catalysts that was approximately one-third the rate of hydrogenolysis. On the other hand, on iridium films, neither Anderson and Avery[23] nor Taylor and Clarke[24] could detect any isomerization of neopentane.

The apparent kinetic parameters obtained from the data shown in Figure 2 at temperatures where a single (two for *n*-butane) C–C bond is cleaved are given in Table II for each of the major reaction channels. At a surface temperature of 475 K, propane and *n*-butane exhibit comparable rates of reaction, whereas ethane and neopentane react more slowly by approximately 1 order of magnitude. However, despite the very different structure of these four hydrocarbons, the apparent rate parameters (for this "low-temperature" linear Arrhenius region) are remarkably similar; i.e. all $k_{app}^{(0)} \cong 10^{13\pm1}$ molecules·site^{-1}·s^{-1} and $E_{app} \cong 34 \pm 3$

(20) The relationship between the carbonaceous residue and the adsorbed reactant intermediates responsible for the major reaction channels is supported also by the kinetic modeling. In particular, for temperatures below the onset of rollover, the kinetic model predicts that the steady-state coverage of the adsorbed intermediate (e.g. $C_3H_6(a)$ for propane) decreases rapidly with decreasing temperatures. For example, for propane on Ir(110)-(1×2), $\theta_{C_3H_6} \propto \exp(-\Delta H^{\ddagger}/k_BT)$, where $\Delta H^{\ddagger} \cong 12$ kcal·mol^{-1} (see Section IV.B). When this value is employed, the steady-state coverage of $C_3H_6(a)$ at 300 K (and P_{HC} = 1 Torr, P_{H_2} = 100 Torr) is calculated to be approximately 2×10^{-4} of the corresponding saturation value. Since our experimental procedure involves terminating the reaction by cooling the catalyst to 300 K, followed by pumping out the reactant/product gas mixture, the postreaction surface analysis will detect only those intermediates that are stable in the reactant mixture at 300 K, i.e. the strongly bound carbonaceous residue. Obviously, this implies that spectroscopic investigations of the adsorbed intermediates responsible for the major reaction channel will be successful only if conducted in situ and under reaction conditions.

(21) Boudart, M.; Ptak, L. D. *J. Catal.* **1970**, *16*, 90.
(22) Foger, K.; Anderson, J. R. *J. Catal.* **1979**, *59*, 325.
(23) Anderson, J. R.; Avery, N. R. *J. Catal.* **1966**, *5*, 446; **1967**, *7*, 315.
(24) Taylor, J. F.; Clarke, J. K. A. *Neue Folge* **1976**, *103*, 216.

Table II. Apparent Kinetic Parameters of Hydrogenolysis[a] on the Ir(111) Surface

reaction temperature range, K	R(475 K),[b] molecules·site^{-1}·s^{-1}	$k_{app}^{(0)}$, molecules·site^{-1}·s^{-1}	E_{app}, kcal·mol^{-1}
	$C_2H_6 + H_2 \rightarrow 2CH_4$		
	1.1×10^{-3}		
450–550		$1.0 \times 10^{13\pm1}$	34.7 ± 2
575–650		$1.4 \times 10^{7\pm1}$	19.7 ± 2
	$C_3H_8 + H_2 \rightarrow CH_4 + C_2H_6$		
	1.0×10^{-2}		
425–450		$4.7 \times 10^{13\pm1}$	33.5 ± 2
500–575		$6.8 \times 10^{9\pm1}$	25.3 ± 2
	$n\text{-}C_4H_{10} + 2H_2 \rightarrow 2CH_4 + C_2H_6$		
	2.7×10^{-2}		
425–500		$7.4 \times 10^{12\pm1}$	31.6 ± 2
525–600		$1.2 \times 10^{8\pm1}$	20.3 ± 2
	neo-$C_5H_{12} + H_2 \rightarrow CH_4 + i\text{-}C_4H_{10}$		
	2.1×10^{-3}		
450–475		$1.2 \times 10^{14\pm1}$	36.4 ± 2
525–600		$1.5 \times 10^{9\pm1}$	25.5 ± 2

[a] Rate parameters were fit to the total conversion by utilizing the expression $R = k_{app}^{(0)} \exp(-E_{app}/k_BT)$. Reactant partial pressures were 1.0 Torr of hydrocarbon and 100 Torr of hydrogen. [b] Reaction rate is in terms of total conversion.

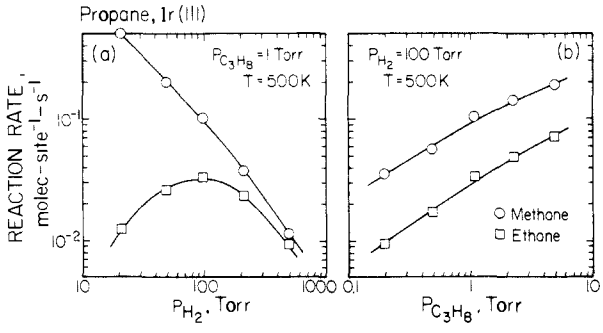

Figure 3. Specific reaction rates for the hydrogenolysis of propane on the Ir(111) surface. (a) The partial pressure of propane was maintained at 1.0 Torr as the partial pressure of hydrogen was varied. (b) The partial pressure of hydrogen was maintained at 100 Torr as the partial pressure of propane was varied.

kcal·mol^{-1}. Depending on the detailed mechanisms of the overall reactions, e.g. the extent of dehydrogenation of the adsorbed reaction intermediates, at this point we cannot rule out the possibility that this agreement is fortuitous. A comparison of these data to those reported previously by Foger and Anderson[22] on a silica-supported iridium catalyst (0.98 wt %, $\bar{d}_{Ir}$ = 70 Å, dispersion of 16% and extrapolated to our reactant partial pressures) is shown in parts a, c, and d of Figure 2, and there is good agreement in all cases. Note, however, the aforementioned restricted temperature range for the data obtained on supported catalysts.

As may be seen in Figure 2, dramatic changes in the selectivity and apparent reaction kinetics occur for propane, *n*-butane, and neopentane as the temperature is increased above approximately 475 K. The apparent activation energy of the rate of conversion decreases,[25] and the selectivity for "complete" hydrogenolysis to methane increases at the expense of the C_{n-1} products. (The simultaneous occurrence of the change in the selectivity and the apparent reaction kinetics is most clearly evident for propane on Ir(110), as may be seen in Figures 9 and 16 below.) Plotted in terms of conversion of the parent hydrocarbon, linear Arrhenius behavior is observed where methane production dominates. Thus, the data for this regime were fit to an Arrhenius expression, and

(25) If one considers the rate of methane production in Figure 2, the decrease in the apparent activation energy seems to occur at a higher temperature compared to that for the change in selectivity. For example, for propane, the rate of conversion of the parent molecule is given by $R_{CH_4}/3 + 2R_{C_2H_6}/3$, for which the break in the reaction kinetics is apparent at 500 K.

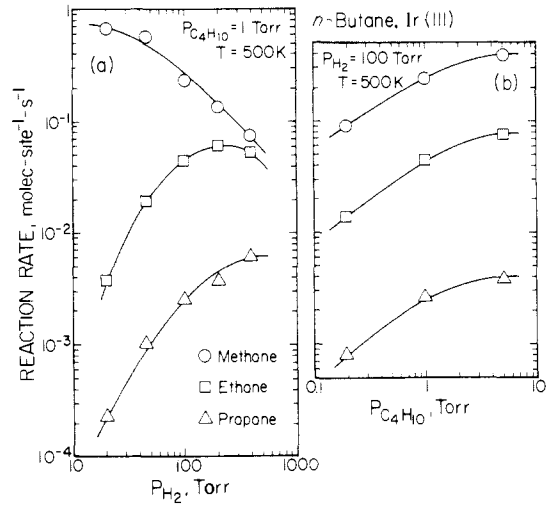

Figure 4. Specific reaction rates for the hydrogenolysis of *n*-butane on the Ir(111) surface. (a) The partial pressure of *n*-butane was maintained at 1.0 Torr as the partial pressure of hydrogen was varied. (b) The partial pressure of hydrogen was maintained at 100 Torr as the partial pressure of *n*-butane was varied.

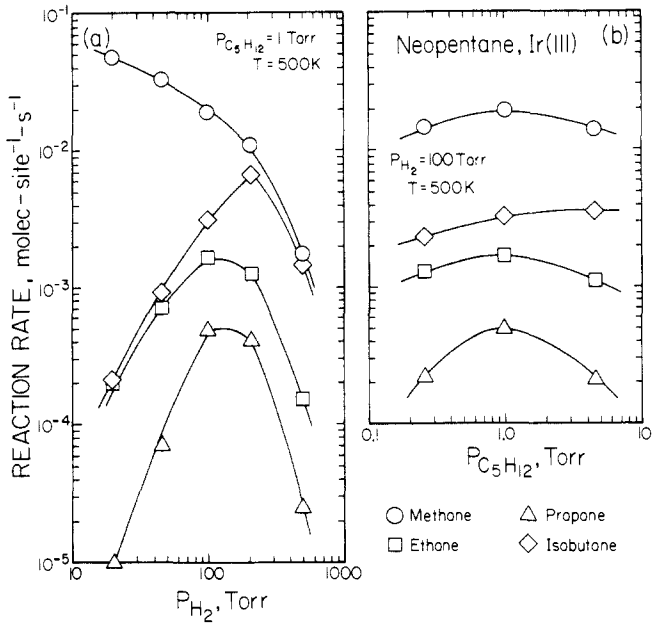

Figure 5. Specific reaction rates for the hydrogenolysis of neopentane on the Ir(111) surface. (a) The partial pressure of neopentane was maintained at 1.0 Torr as the partial pressure of hydrogen was varied. (b) The partial pressure of hydrogen was maintained at 100 Torr as the partial pressure of neopentane was varied.

the apparent kinetic parameters are given in Table II. In this "high-temperature" regime, for these four hydrocarbons, the apparent kinetic parameters are again quite similar, given by values of $k_{app}^{(0)} \cong 3 \times 10^{8\pm1.5}$ molecules·site^{-1}·s^{-1} and $E_{app} \cong 22 \pm 3$ kcal·mol^{-1}.

The transition region between the low- and high-temperature linear Arrhenius regions, corresponding to changes in both the apparent kinetics and the selectivity, which we shall designate as "rollover", can be identified explicitly with a depletion in the steady-state coverage of hydrogen adatoms by varying the hydrogen partial pressure at a temperature near the onset of the break in the apparent reaction kinetics. In order to assess various mechanistic models, it is also necessary to vary the hydrocarbon partial pressure. Therefore, reaction rates were measured for variations in both the hydrogen and hydrocarbon partial pressures, while maintaining a constant partial pressure of the other and a constant temperature. These data are shown in Figures 3–5 for propane, *n*-butane, and neopentane, respectively. It is important

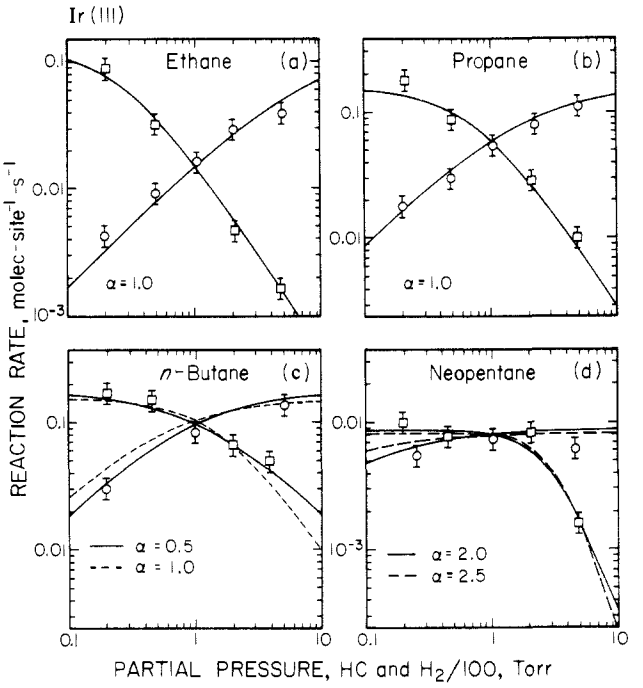

Figure 6. Analytic fits of the measured specific reaction rates in terms of conversion (parent molecules·site^{-1}·s^{-1}) to eq **4** for (a) ethane, (b) propane, (c) *n*-butane, and (d) neopentane on the Ir(111) surface at 500 K. The circles represent experimental data for which the partial pressure of hydrogen was maintained at 100 Torr as the partial pressure of the hydrocarbon was varied. The squares represent experimental data for which the partial pressure of hydrocarbon was maintained at 1.0 Torr as the partial pressure of the hydrogen was varied. The central data point, corresponding to the "standard" reactant partial pressures (P_{HC} = 1 Torr and P_{H_2} = 100 Torr), applies to both curves. The optimal, statistically significant values of α are displayed in each case.

to note that the coverages of the carbonaceous residue remained essentially identical with those given in Table I, as the partial pressures were varied. Thus, any changes observed in the activity and/or selectivity cannot be associated with the carbonaceous residue (e.g. "self-poisoning") and must be due to variations in the coverages of the adsorbed reactants associated with the major reaction channels. As may be seen in Figures 3–5, a reduction in the hydrogen partial pressure near the onset of rollover has the same effect as an increase in the temperature; i.e., the selectivity for methane increases greatly. Since both reducing the hydrogen partial pressure and increasing the surface temperature result in a decrease in the hydrogen coverage, *rollover is clearly associated with a depletion in surface hydrogen.*

A number of qualitative features of the dependence of the specific rates of hydrogenolysis on the reactant partial pressures are apparent in parts a–d of Figure 6, where the specific rates are plotted in terms of total conversion of the parent alkane. In all cases, the apparent reaction "order" (i.e. $\partial(\ln R)/\partial(\ln P_{HC})$) lies between 1 and 0 and decreases as P_{HC} is increased. On the other hand, the order in the hydrogen partial pressure is ≤ 0 and decreases as P_{H_2} is increased. Similar behavior has been reported, for example, for ethane hydrogenolysis on a number of supported group VIII metal catalysts.[2] Returning to Figures 3–5, the sensitivity of the selectivity of hydrogenolysis is quite different. In particular, the selectivity is essentially independent of P_{HC}, whereas at low P_{H_2} the selectivity for the production of C_{n-1} (C_{n-2} for *n*-butane) hydrocarbons decreases sharply as P_{H_2} is reduced.

A quantitative analysis of the data shown in Figures 3–6 is possible when a mechanisitic scheme similar to those proposed previously by Cimino et al.[15] and by Sinfelt[16] is employed. The major assumptions of the model employed here, which is described in detail elsewhere,[26] may be summarized as follows: (1) pseudoequilibrium is maintained between the gas-phase reactants and a partially dehydrogenated hydrocarbon fragment (the carbon skeleton of which remains intact) and the adsorbed hydrogen adatoms; (2) the rate-limiting step involves an irreversible carbon–carbon bond cleavage in the partially dehydrogenated hydrocarbon fragments; and (3) hydrogenation of the resulting fragments (or additional C–C bond cleavage and subsequent hydrogenation) is rapid with respect to the initial C–C bond cleavage reaction. Assumption 1 involves the following set of reactions

$$C_nH_{2n+2}(g) \rightleftarrows C_nH_x(a) + 2\alpha H(a) \quad (1)$$

$$H_2(g) \rightleftarrows 2H(a) \quad (2)$$

where $\alpha \equiv (2n + 2 - x)/2$. Note that "reaction" 1 embodies one ($\alpha = {}^1/_2$) or more ($\alpha \geq 1$) elementary steps. Assumption 2 involves the reaction

$$C_nH_x(a) \rightarrow C_mH_y(a) + C_{n-m}H_z(a) \quad (3)$$

where $x = y + z$, and the resulting fragments, $C_mH_y(a)$ and $C_{n-m}H_z(a)$, are subsequently hydrogenated rapidly.

The analysis of the mechanistic scheme of eq 1–3, which is presented elsewhere,[26] results in the following expression for the total rate of hydrogenolysis (i.e. conversion of the parent hydrocarbon) as a function of the partial pressures of the reactants (eq 4) where $k_C(T)$ is the rate coefficient of the elementary reaction

$$R_C = k_C\theta_{C_nH_x} = \frac{k_C K^* P_{HC}}{K^* P_{HC} + P_{H_2}{}^{\alpha+1/2}} \quad (4)$$

given by eq 3, $\theta_{C_nH_x}$ is the (temperature and partial pressure dependent) fractional coverage of the $C_nH_x(a)$ species, and $K^*(T)$ is a combination of rate coefficients of the reactions given in eq 1 and 2 (defined explicitly elsewhere[26]). Note that eq 4 predicts that the apparent order of the reaction in the hydrocarbon partial pressure will vary from 1 to 0 as P_{HC} is increased, whereas that for hydrogen will vary from 0 to $-(\alpha + {}^1/_2)$ as P_{H_2} is increased, consistent with the experimental observations (especially if the four reactions are viewed as a set). Consequently, in principle, the stoichiometry of the adsorbed parent hydrocarbon fragment (i.e. $x = 2(n - \alpha) + 2$) can be determined by varying the reactant partial pressures.

The major difference between the expression derived here (eq 4) and those derived previously[15,16] is the presence of an additional power of ${}^1/_2$ in the partial pressure of hydrogen. This is due to our including competition of the reactants for adsorption sites; i.e., hydrogen adatoms can block the dissociative adsorption and further dehydrogenation of the parent alkane by occupying surface sites.[27] If one neglects this site blocking by hydrogen, one would overestimate the extent of dehydrogenation of the reaction intermediate by one hydrogen atom.

The data shown in parts a–d of Figure 6 have been fit to the functional form given by eq 4. The optimal parameters were obtained utilizing a least-squares functional minimization routine based on a simplex method[28] where, initially, the constant α was allowed to vary arbitrarily (i.e. it was not constrained to half-integral values). Subsequently, the data were refit by fixing α to the two nearest half-integral values, and the set of parameters that produced the best, statistically significant fit were judged to be the optimal parameters. The agreement between the data and the behavior predicted by eq 4 is excellent and within experimental error, as may be seen from Figure 6. In all cases the dimensionless standard deviation between the model and the data is less than approximately 20%. The stoichiometries for the adsorbed hydrocarbon fragments that are implied by these data are summarized in Table III. Consistent with the proposition that hydrogenolysis proceeds through a partially dehydrogenated intermediate that is multiply bound to the surface by one or more metal

(26) A detailed description of the mechanistic model employed here, represented by eq 4, 7, and 11, is available as supplementary material.

(27) Wittrig, T. S.; Szuromi, P. D.; Weinberg, W. H. *J. Chem. Phys.* **1982**, *76*, 3305.

(28) Nedler, J. A.; Mead, R. *Comput. J.* **1965**, *7*, 308.

Table III. Apparent Reaction Intermediates[a] on the Ir(111) Surface

reactant, $C_nH_{2n+2}(g)$	parent fragment, $C_nH_x(a)$	product fragment, $C_mH_y(a)$
C_2H_6	C_2H_4	
C_3H_8	C_3H_6	C_2H_2
n-C_4H_{10}	C_4H_8 or C_4H_9	C_2H_1
neo-C_5H_{12}	C_5H_7 or C_5H_8	C_4H_5 or C_4H_6

[a] Reaction mechanism is given by the following (also see text): $C_nH_{2n+2}(g) \rightleftarrows C_nH_x(a) + 2\alpha H(a)$, $C_nH_x(a) \rightarrow C_mH_y(a) + C_{n-m}H_z(a)$, and $C_mH_y(a) + 2\beta H(a) \rightarrow C_mH_{2m+2}(g)$.

atoms, in all cases (with the possible exception of *n*-butane) at least two hydrogen atoms are removed from the parent molecule.

The success of applying the mechanistic model described by eq 1–3 to the experimental data permits an interpretation of the rollover phenomena via the use of eq 4. At high partial pressures of hydrogen, $P_{H_2}^{\alpha+1/2} \gg K^* P_{HC}$, and the reaction rate is given by $k_C K^* P_{HC}/P_{H_2}^{\alpha+1/2}$. Thus, the apparent activation energy is given by $E_{app} \cong E_C + \Delta H^*$, where E_C is the activation energy of the C–C bond cleavage reaction of eq 3, and ΔH^* is the total enthalpy change for the set of reactions given by $C_nH_{2n+2}(g) + H(a) \rightarrow C_nH_x(a) + (\alpha + {}^1/_2)H_2(g)$.[29] However, as the partial pressure of hydrogen is reduced to an extent such that $P_{H_2}^{\alpha+1/2} \ll K^* P_{HC}$, the reaction rate is given by k_C, and the apparent activation energy is given by $E_{app} \cong E_C$. Associating temperatures below rollover with high hydrogen partial pressures and temperatures above rollover with low pressures would imply that the enthalpy change ΔH^* is positive, since rollover is accompanied by a decrease in the apparent activation energy (with respect to conversion).

Support for this proposal can be obtained by determining the apparent reaction orders in the reactant partial pressures at different temperatures (i.e. by similarly varying the reactant partial pressures at different temperatures). For example, over Ir blacks under similar reaction conditions,[30] the apparent order in P_{H_2} for ethane hydrogenolysis was found to increase continuously with temperature from approximately $-1^1/_2$ at 450 K to approximately $-{}^1/_2$ at 575 K. This experimental observation implies that the coefficient K^* increases with temperature (where $K^*(T) = K^{*(0)} \exp(-\Delta H^*/k_B T)$), and therefore ΔH^* must be positive (i.e. if $K^* P_{HC} \ll P_{H_2}^{\alpha+1/2}$, the order in P_{H_2} approaches $-(\alpha + {}^1/_2)$, whereas if $K^* P_{HC} \gg P_{H_2}^{\alpha+1/2}$, the order in P_{H_2} approaches zero).

A rigorous test of the physical significance of the mechanistic model proposed here can be obtained by comparing the measured apparent preexponential factors to those predicted theoretically by employing physically reasonable preexponential factors.[26] In particular, in the "high-temperature" regime, eq 4 predicts that the apparent preexponential factor will be given by $k_C^{(0)}\theta_{C_nH_x(sat)}$, where $k_C^{(0)}$ is the preexponential factor for the reaction of eq 3 and $\theta_{C_nH_x(sat)}$, is the saturation coverage of the dissociatively adsorbed intermediate. Separate experiments on *clean* surfaces of iridium[27] indicate that $\theta_{C_nH_x(sat)} \cong 0.05$; however, in the presence of the carbonaceous residue, this value is most assuredly too large, i.e. a value of 0.03 is more reasonable. Thus, assuming $k_C^{(0)} \cong 10^{12\pm2}$ s^{-1} the predicted apparent preexponential is given by $3 \times 10^{10\pm2}$ s^{-1}. Examination of Table II (and Table V for Ir(110)-(1×2), see below) shows excellent agreement between the measured and predicted values.

In the low-temperature regime, the apparent preexponential factor predicted by eq 4 is given by $k_C^{(0)} K^{*(0)} P_{HC}/P_{H_2}^{\alpha+1/2}$; i.e., it is function of α, which is proportional to the extent of dehydrogenation of the dissociatively adsorbed intermediate. In this case, in order to compare the measured and predicted values, we shall consider the ratio of the low- and high-temperature apparent preexponential factors, which is given by $K^{*(0)} P_{HC}/P_{H_2}^{\alpha+1/2}$. When physically reasonable preexponential factors (i.e. $10^{12\pm2}$ s^{-1}) and the calculated impingement rates of the gas-phase reactants[26] are employed the predicted value is given by $0.3 \times 10^{0\pm4} \times (1.7 \times 10^4)^{\alpha-1}$. The measured values for this ratio (cf. Table II) vary from $7 \times 10^{3\pm2}$ to $7 \times 10^{5\pm2}$, which, given the experimental uncertainties, are in reasonable agreement with the predicted value. Most importantly, for a given reaction, the mechanism predicts that this ratio should increase with the extent of dehydrogenation of the adsorbed intermediate, i.e. α.

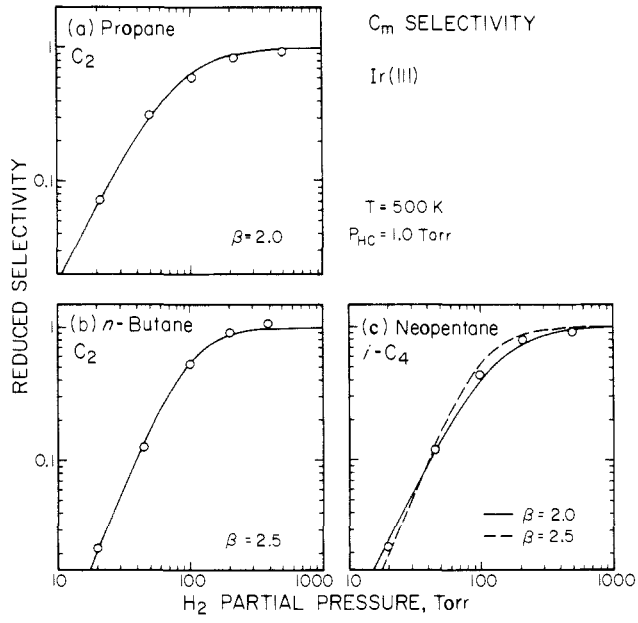

Figure 7. Analytic fits of the C_m selectivity, with respect to C_n conversion, to eq 7 for (a) propane, (b) *n*-butane, and (c) neopentane on the Ir(111) surface. In all cases the partial pressure of the hydrocarbon was 1.0 Torr. The optimal, statistically significant values of β are displayed in each case.

The data shown in Figure 3–5 can be utilized to interpret the changes observed in the selectivities in the rollover regime. For example, propane reacts to form a C_2 and a C_1 species via the reaction of eq 3. If sufficient hydrogen adatoms are present, these species will be hydrogenated rapidly, producing ethane and methane. However, if the hydrogen adatom concentration is depleted, as is the case in the rollover regime, the C_2 species could react further with the surface to produce two C_1 species and, eventually, methane. We can describe this situation by employing a scenario similar to that given by eq 1–3, except in this case for the C_2 species. Thus, we shall consider reactions 5 and 6 where

$$C_mH_y(a) + 2\beta H(a) \rightleftarrows C_mH_{2m+1}(a) + H(a) \rightarrow C_mH_{2m+2}(g) \quad (5)$$

$$C_mH_y(a) \rightarrow C_1H_u(a) + C_{m-1}H_v(a) \quad (6)$$

$\beta = (2m + 2 - y')/2$ and $y' = u + v$. In this case, we have neglected secondary reactions of the gas-phase C_mH_{2m+2} product, clearly valid at low conversions. Proceeding in a similar fashion as in the derivation of eq 4,[26] we find that the C_m selectivity with respect to the total C_n conversion at a constant temperature is given by eq 7 where $k_S(T)$ represents a combination of rate coefficients,

$$S_{C_m} \equiv R_{C_m}/R_C = k_S P_{H_2}^{\beta}/(1 + k_S P_{H_2}^{\beta}) \quad (7)$$

given elsewhere.[26] Note that, in agreement with the experimental observations, this selectivity is not a function of P_{HC}. It is also important to note that y' of eq 5 is not necessarily equal to y of eq 3. Subsequent to the initial C–C bond cleavage, the C_m species may dehydrogenate further prior to additional C–C bond cleavage. Thus, y' of eq 5 will provide a minimum value for y of eq 3, whereas x obviously represents the maximum value. In evaluating the minimum limiting value of y, we exclude the possibility that additional C–C bond cleavage could be preceded by a hydro-

(29) By writing the set of reactions as $C_nH_{2n+2}(g) + H(a) \rightarrow C_nH_x(a) + (\alpha + {}^1/_2)H_2(g)$, we do not mean to imply an elementary reaction between the gas-phase hydrocarbon and a hydrogen adatom. On the contrary, the proper interpretation is that a hydrogen adatom must be desorbed in order to create a vacant site to facilitate the chemisorption and/or dehydrogenation of the hydrocarbon.

(30) Sarkany, A.; Matusek, K.; Tetenyi, P. *J. Chem. Soc., Faraday Trans. 1* **1977**, *73*, 1699.

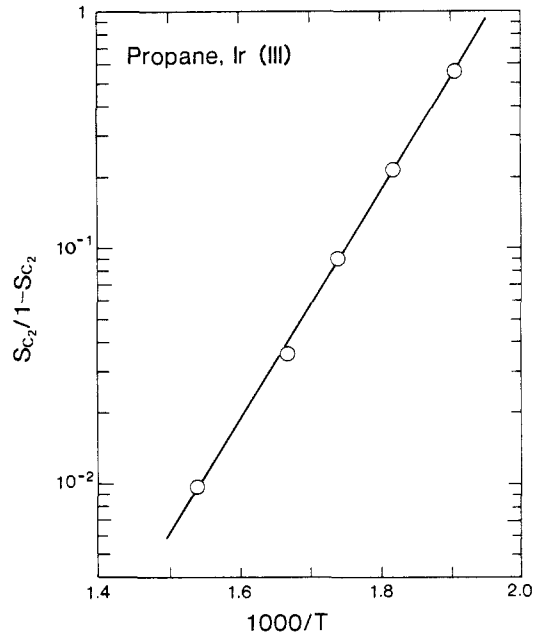

Figure 8. Selectivity function $S_{C_2}/(1 - S_{C_2})$ concerning the production of ethane from propane on the Ir(111) surface plotted versus reciprocal temperature. The partial pressure of propane was 1.0 Torr and that of hydrogen was 100 Torr.

genation step. Note that if y were determined exactly by eq 7 (i.e. if $y = y'$), the stoichiometry of eq 3 would be completely specified, since x is determined independently from eq 4.

The data presented in Figures 3a–5a for propane, *n*-butane, and neopentane have been fit to eq 7 by utilizing a least-squares routine similar to that described above. The results are shown in parts a–c of Figure 7. We see that the data are described well by this model. In all cases, the standard deviation between the data and this model is less than approximately 10%. The (minimum) hydrogen content of the C_m fragments implied by these data is summarized in Table III.

A consistency check for our analysis of the variation of the selectivity with changing reactant partial pressures via the use of eq 7 can be obtained if we consider the temperature dependence of the selectivity. In particular, as discussed elsewhere,[26] $k_s(T)$ represents a multiplicative combination of rate coefficients. Consequently, an Arrhenius plot of the quantity $S_{C_m}/(1 - S_{C_m})$ should be linear, and its slope (intercept) will be given by a combination of activation barriers (preexponential factors). An Arrhenius plot of $S_{C_2}/(1 - S_{C_2})$ vs reciprocal temperature for the reaction of propane on the Ir(111) surface is shown in Figure 8. The expected linearity is evident, which, in this case, results in an apparent activation energy of −22.2 kcal·mol^{-1} and an apparent preexponential factor of 3.3×10^{-10}. Linear Arrhenius behavior is observed also for *n*-butane and neopentane. In regards to the physical significance of eq 7, when preexponential factors for the elementary surface reactions of $10^{12\pm2}$ s^{-1} are employed, the predicted value for the apparent preexponential factor for this reaction at $P_{H_2} = 100$ Torr is $3.3 \times 10^{-9\pm4}$, which is in excellent agreement with the measured value.

B. Ir(110)-(1×2) Surface. Specific rates of hydrogenolysis of ethane, propane, *n*-butane, and neopentane on the Ir(110)-(1×2) surface are shown in parts a–d of Figure 9 in Arrhenius form. These data represent steady-state reaction rates, obtained for conversions that were restricted typically to below 1%. The standard reactant partial pressure ratio, H_2/C_nH_{2n+2}, was 100/1, with a hydrocarbon partial pressure of 1.0 Torr.

Postreaction surface characterization by Auger electron spectroscopy indicated the presence of a submonolayer carbonaceous residue on the Ir(110)-(1×2) surface. The measured values for the fractional coverages, which in all cases considered here and below were essentially independent of reaction conditions (surface temperature and reactant partial pressures), are given in Table

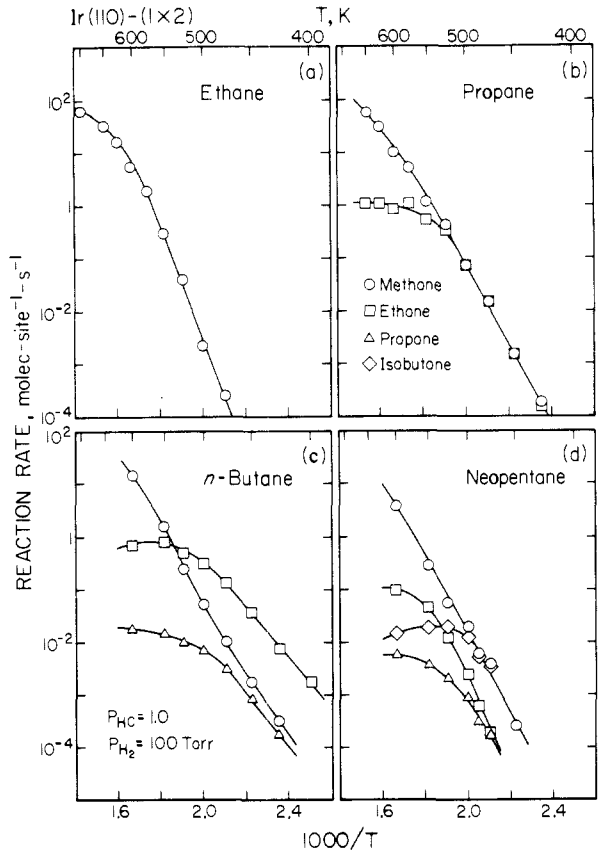

Figure 9. Specific reaction rates (product molecules·site^{-1}·s^{-1}) for the hydrogenolysis of (a) ethane, (b) propane, (c) *n*-butane, and (d) neopentane on the Ir(110)-(1×2) surface. The partial pressure of hydrocarbon was 1.0 Torr, whereas that of hydrogen was 100 Torr.

Table IV. Carbonaceous Residue Following Hydrogenolysis Reactions on the Ir(110)-(1×2) Surface

reactant	fractional carbon coverage, θ_C
ethane	0.18 ± 0.07
propane	0.21 ± 0.04
n-butane	0.24 ± 0.08
neopentane	0.44 ± 0.13

IV in terms of fractional carbon coverage. As was observed on the Ir(111) surface, there is an approximately linear increase in the carbon coverage with increasing size of the parent hydrocarbon. Furthermore, the fractional coverages observed on each surface are very similar to one another (cf. Tables I and IV). These similarities tend to rule out the possibility that sites unique to the (110)-(1×2) surface are poisoned selectively. On the other hand, if activity and/or selectivity differences are observed between these two surfaces for a particular reaction, it is unlikely that these differences are due to a particular configuration of the carbonaceous residue present on each of the surfaces. Postreaction thermal desorption from the carbonaceous overlayer produced only H_2, and the resulting desorption spectra were similar to those observed from the (111) surface. Titration of the carbonaceous overlayer with hydrogen produced only methane in all cases, which, as discussed above in Section III.A, suggests that the carbonaceous residue is not representative of the adsorbed intermediates associated with the major reaction channels.

As with the Ir(111) surface, the only reaction products observed were methane, ethane, propane, and isobutane. No isomerization products were detected from either *n*-butane or neopentane (where we must qualify our estimates for the maximum rates of isomerization as for the (111) surface; see Section III.A). With the exception of *n*-butane, the major reaction channels at sufficiently low temperatures ($T \leq 500$ K) are given by

$$C_nH_{2n+2} + H_2 \rightarrow CH_4 + C_{n-1}H_{2(n-1)+2}$$

Table V. Apparent Kinetic Parameters of Hydrogenolysis[a] on the Ir(110)-(1×2) Surface

reaction temperature range, K	R(475 K),[b] molecules·site^{-1}·s^{-1}	$k_{app}^{(0)}$, molecules·site^{-1}·s^{-1}	E_{app}, kcal·mol^{-1}
	$C_2H_6 + H_2 \rightarrow 2CH_4$		
	1.3×10^{-4}		
475–575		$5.8 \times 10^{18\pm1}$	49.4 ± 2
575–700		$2.4 \times 10^{9\pm1}$	22.8 ± 2
	$C_3H_8 + H_2 \rightarrow CH_4 + C_2H_6$		
	1.5×10^{-2}		
425–525		$1.2 \times 10^{14\pm1}$	34.7 ± 2
525–650		$8.4 \times 10^{8\pm1}$	22.6 ± 2
	$n\text{-}C_4H_{10} + 2H_2 \rightarrow 2C_2H_6$		
	7.8×10^{-2}		
400–475		$1.1 \times 10^{9\pm1}$	22.2 ± 2
	neo-$C_5H_{12} + H_2 \rightarrow CH_4 + i\text{-}C_4H_{10}$		
	4.2×10^{-3}		
450–500		$6.2 \times 10^{13\pm1}$	35.6 ± 2
500–600		$4.6 \times 10^{8\pm1}$	24.1 ± 2

[a] Rate parameters were fit to the total conversion by utilizing the expression $R = k_{app}^{(0)} \exp(-E_{app}/k_BT)$. Reactant partial pressures were 1.0 Torr of hydrocarbon and 100 Torr of hydrogen. [b] Reaction rate is in terms of total conversion.

For *n*-butane on Ir(110)-(1×2), the major reaction channel is given by

$$n\text{-}C_4H_{10} + H_2 \rightarrow 2C_2H_6$$

Of the four reactions on the two surfaces considered here, the hydrogenolysis of *n*-butane on the Ir(110)-(1×2) surface is the only one that does not produce methane from the major reaction channel. Hence, the *selectivity* for the hydrogenolysis of *n*-butane by iridium catalysts is sensitive to the structure of the surface.

The apparent kinetic parameters derived from the data shown in Figure 9 are given in Table V for each of the major reaction channels. At a common temperature of 475 K the reaction rates in terms of conversion may be ordered as follows: *n*-butane > propane > neopentane > ethane. In addition, unlike the Ir(111) surface, the apparent reaction rate parameters differ considerably for the low-temperature linear Arrhenius region for the four hydrocarbons. Specifically, the parameters for the hydrogenolysis of ethane are given by $k_{app}^{(0)} \cong 6 \times 10^{18}$ molecules·site^{-1}·s^{-1} and $E_{app} \cong 49 \pm 2$ kcal·mol^{-1}; those for propane and neopentane are similar to one another and are given by $k_{app}^{(0)} \cong 1 \times 10^{14}$ molecules·site^{-1}·s^{-1} and $E_{app} \cong 35 \pm 2$ kcal·mol^{-1}; and those for *n*-butane are given by $k_{app}^{(0)} \cong 1 \times 10^{9}$ molecules·site^{-1}·s^{-1} and $E_{app} \cong 22 \pm 2$ kcal·mol^{-1}. It is of interest to note that the values obtained on the (111) and (110)-(1×2) surfaces for the hydrogenolysis of propane and neopentane are nearly indistinguishable. However, both the apparent activation energy and preexponential factor for ethane hydrogenolysis are much greater on the (110)-(1×2) surface, whereas those for *n*-butane hydrogenolysis are considerably smaller with respect to those observed on the (111) surface. These results suggest that different intermediates may exist on the two surfaces for these two reactions.

Consistent with the observations on the Ir(111) surface, dramatic changes in the selectivity and apparent reaction kinetics occur for propane, *n*-butane, and neopentane hydrogenolysis on the (110)-(1×2) surface as the temperature is increased above approximately 500 K. Again, these rollover phenomena are associated with a depletion in the steady-state coverage of hydrogen. Moreover, when the results obtained on the two surfaces are compared, the source of the hydrogen can be identified explicitly. For example, the relative selectivity for ethane with respect to methane from the hydrogenolysis of propane, i.e. $R_{C_2H_6}/R_{CH_4}$, is approximately equal to $^1/_3$ at 500 K on Ir(111) and at 550 K on Ir(110)-(1×2) (cf. Figures 2b and 9b). Since our results implicate the presence of similar intermediates on both surfaces for this reaction (see below; Tables III and VI), the observed difference in the onset of rollover is due primarily to differing energetics of the chemisorbed hydrogen. Consequently, since rollover occurs at a higher temperature on the Ir(110)-(1×2) surface, this surface must possess hydrogen adsites characterized by a higher binding energy than those available on the (111) surface. Independent measurements of the adsorption and desorption kinetics of hydrogen on clean (111) and (110)-(1×2) surfaces of Ir have verified the expected presence of a higher binding energy adstate on the (110)-(1×2) surface.[19] The agreement between these results obtained on clean surfaces and those obtained here under reaction conditions (i.e. both implicating hydrogen being more strongly bound on the (110)-(1×2) surface) points to the surface metal atoms as the source of the hydrogen. This identification precludes (as the mechanism embodied by eq 4 does implicitly), for example, any mechanism involving the carbonaceous overlayer acting as a "hydrogen-transfer agent".

Table VI. Apparent Reaction Intermediates[a] on the Ir(110)-(1×2) Surface

reactant, C_nH_{2n+2}(g)		parent fragment, C_nH_x(a)	product fragment, C_mH_y(a)
C_2H_6		C_2H_2	
C_3H_8		C_3H_6	C_2H_1 or C_2H_2
$n\text{-}C_4H_{10}$	major	C_4H_8	C_2H_4
	minor	C_4H_8 or C_4H_9	C_3H_4 or C_3H_5
neo-C_5H_{12}		C_5H_7 or C_5H_8	C_4H_5 or C_4H_6

[a] Reaction mechanism is given by the following (also see text): $C_nH_{2n+2}(g) \rightleftarrows C_nH_x(a) + 2\alpha H(a)$, $C_nH_x(a) \rightarrow C_mH_y(a) + C_{n-m}H_z(a)$, $C_mH_y(a) + 2\beta H(a) \rightarrow C_mH_{2m+2}(g)$. For the major channel of *n*-butane, the second reaction (C–C bond cleavage) is reversible, and $y = y'$, $m = n/2$, and $y = x/2$.

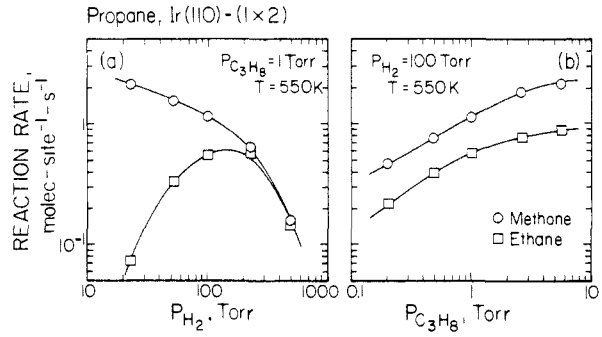

Figure 10. Specific reaction rates for the hydrogenolysis of propane on the Ir(110)-(1×2) surface. (a) The partial pressure of propane was maintained at 1.0 Torr as the partial pressure of hydrogen was varied. (b) The partial pressure of hydrogen was maintained at 100 Torr as the partial pressure of propane was varied.

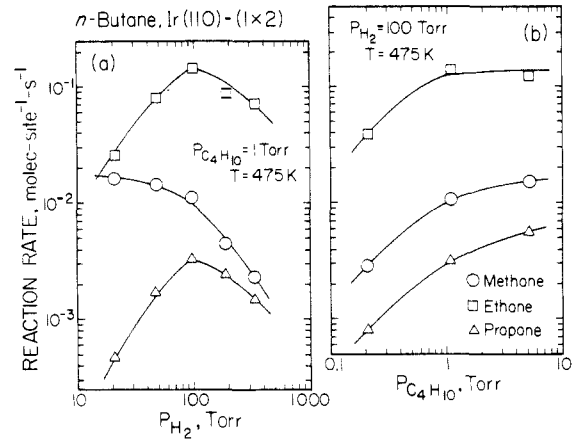

Figure 11. Specific reaction rates for the hydrogenolysis of *n*-butane on the Ir(110)-(1×2) surface. (a) The partial pressure of *n*-butane was maintained at 1.0 Torr as the partial pressure of hydrogen was varied. (b) The partial pressure of hydrogen was maintained at 100 Torr as the partial pressure of *n*-butane was varied.

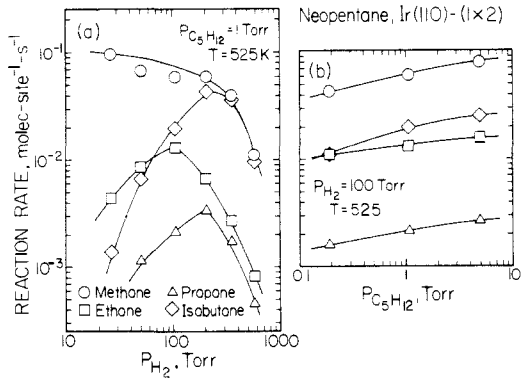

Figure 12. Specific reaction rates for the hydrogenolysis of neopentane on the Ir(110)-(1×2) surface. (a) The partial pressure of neopentane was maintained at 1.0 Torr as the partial pressure of hydrogen was varied. (b) The partial pressure of hydrogen was maintained at 100 Torr as the partial pressure of neopentane was varied.

Verification of the role of hydrogen in the rollover phenomena was again provided by varying the partial pressures of the reactants at a temperature near the onset of rollover. These data for the Ir(110)-(1×2) surface are shown in Figures 10–12 for propane, *n*-butane, and neopentane. As was found on the Ir(111) surface, for all reaction conditions considered in Figures 10–12, the coverages of the carbonaceous residue were essentially identical with those given in Table IV. A reduction in the partial pressure of hydrogen has the same effect as an increase in the temperature for propane and neopentane; namely, the selectivity for methane increases greatly. However, for *n*-butane, a reduction in the hydrogen partial pressure results in a decrease in the total rate of *conversion*; e.g., as P_{H_2} is reduced from 100 to 20 Torr, the total rate of conversion of *n*-butane decreases by a factor of approximately 5. In this case, unlike propane and neopentane, the decrease in the rate of production of ethane is *not* compensated by a corresponding increase in the rate of production of methane (i.e. conversion of *n*-butane to ethane dominates for all P_{H_2} displayed in Figure 11; even at 20 Torr of H_2, conversion to ethane is approximately a factor of 4 times that to methane). Rather, in this case, the slight increase in methane production with decreasing P_{H_2} is probably associated with the corresponding decrease in the propane production. These observations suggest that two distinct reaction pathways are operating simultaneously for *n*-butane on Ir(110)-(1×2); the major pathway is $n\text{-}C_4H_{10} + H_2 \rightarrow 2C_2H_6$, whereas the minor one is $n\text{-}C_4H_{10} + H_2 \rightarrow CH_4 + C_3H_8$.

The observed positive order in P_{H_2} for the rate of conversion of *n*-butane for pressures below 100 Torr (observed also for neopentane to a lesser extent, see below) might be explained by either of the following: (1) surface hydrogen is participating in the C–C bond cleavage reaction of eq 4 (i.e. the reaction is "bimolecular") or (2) the C–C bond cleavage reaction is reversible (i.e. overall, hydrogenolysis is positive order in P_{H_2}). The plausibility of these two explanations is considered below.

The data shown in Figure 10 for propane and similar data for ethane have been fit to the functional form of eq 4. These data are shown in parts a and b of Figure 13, where the standard deviation in both cases is less than approximately 20%. The stoichiometries of the adsorbed reaction intermediates implied by these data are summarized in Table VI. Note that the stoichiometry of the intermediate for propane is identical with that observed on the Ir(111) surface, which together with the similarities between the apparent kinetics suggests that similar pathways may exist on both surfaces for this reaction.

The data presented in Figure 12 for neopentane are plotted in Figure 13d in terms of total conversion. For partial pressures below approximately 200 Torr, the apparent order in P_{H_2} is positive and nearly equal to $^1/_2$. This small positive order in P_{H_2} can be rationalized if the rate-limiting C–C bond cleavage of eq 3 involves a bimolecular reaction between the hydrocarbon fragment and a hydrogen adatom (i.e. $R_C = k_C\theta_{C_nH_x}\theta_H$).[31] When the mechanistic scheme detailed elsewhere[26] is employed, it can be shown that if one assumes that C–C bond cleavage involves a bimolecular reaction with a hydrogen adatom, the resulting expression for the rate of hydrogenolysis is given by a form similar to eq 4, but with the essential difference that there is an additional factor of $P_{H_2}^{1/2}$ in the numerator. Consequently, the data for neopentane have been fit to the product of the expression given in eq 4 and $P_{H_2}^{1/2}$. The data for neopentane are fit equally well by values for α of 2 and $2^1/_2$, the standard deviation being 23% in both cases. Note that, as with propane, the stoichiometries of the apparent reaction intermediates from neopentane on the two surfaces are identical with each other (cf. Tables III and VI).

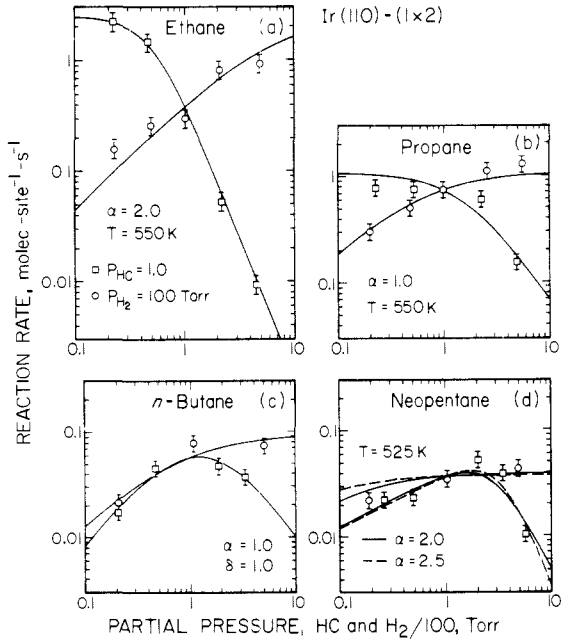

Figure 13. Analytic fits of the specific reaction rates in terms of conversion (parent molecules·site^{-1}·s^{-1}) to eq 4 for (a) ethane, (b) propane, and (d) neopentane and to eq 11 for (c) *n*-butane on the Ir(110)-(1×2) surface. The circles represent the cases for which the partial pressure of hydrogen was maintained at 100 Torr as the partial pressure of the hydrocarbon was varied. The squares represent the cases for which the partial pressure of hydrocarbon was maintained at 1.0 Torr as the partial pressure of the hydrogen was varied. The central data point, corresponding to the standard reactant partial pressures (P_{HC} = 1 Torr and P_{H_2} = 100 Torr), applies to both curves. The optimal, statistically significant values of α are displayed in each case. The data for neopentane were fit to a modified form of eq 4, namely, the product of the expression given by eq 4 and $k_bP_{H_2}^{1/2}$, where k_b is a constant coefficient (see text).

The data presented in Figure 11 for *n*-butane are plotted in Figure 13c in terms of total conversion. As discussed above in connection with Figure 11, the apparent order in P_{H_2} is positive and is approximately equal to unity for partial pressures of hydrogen below 100 Torr. However, unlike neopentane, it is difficult to reconcile a positive order in P_{H_2} of unity in terms of hydrogen participating in the C–C bond cleavage reaction (i.e. it implicates a third-order reaction). On the other hand, since hydrogenolysis does involve the incorporation of hydrogen, i.e. "overall" it is positive order in P_{H_2} (e.g. $C_4H_{10} + H_2 \rightarrow 2C_2H_6$), one possible interpretation of this result is that C–C bond cleavage is reversible;

(31) Another possible explanation for the observed small positive order in P_{H_2} is that the initial C–C bond cleavage reaction of eq 3 is no longer rate-limiting. In particular, for neopentane, a reduction in P_{H_2} increases the selectivity for methane production greatly; i.e., multiple C–C bond cleavage becomes the dominant pathway. If the "secondary" C–C bond cleavage reactions (and subsequent hydrogenations) are not rapid with respect to the initial C–C bond cleavage reaction, these secondary reactions can limit the overall rate of reaction. For example, if the coverages of the product fragments become significant, their presence on the surface can block the dissociative adsorption of the parent hydrocarbon. The fact that "complete" hydrogenolysis of neopentane involves the scission of four C–C bonds, as opposed to two for propane, suggests that this interpretation may be important for neopentane.

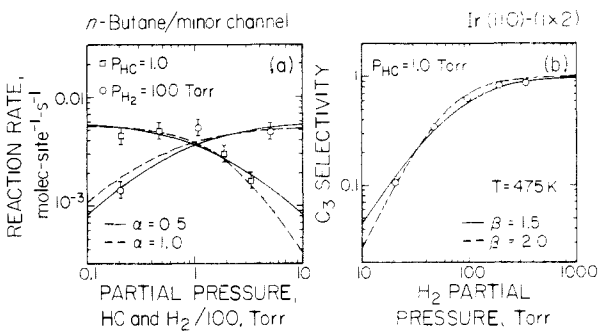

Figure 14. Analytic fits of (a) the specific reaction rate to eq 4 and (b) the C_3 selectivity to eq 7 for the minor reaction channel of *n*-butane hydrogenolysis on the Ir(110)-(1×2) surface; i.e., $n\text{-}C_4H_{10} + H_2 \rightarrow CH_4 + C_3H_8$. The optimal, statistically significant values of α and β are displayed in each case.

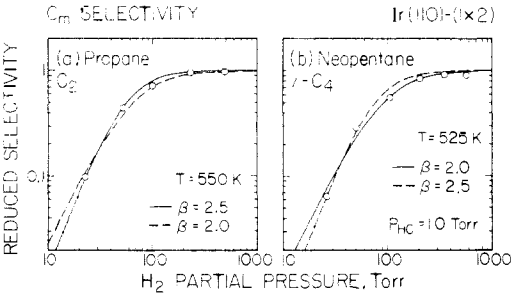

Figure 15. Analytic fits of the C_m selectivity, with respect to C_n conversion, to eq 7 for (a) propane and (b) neopentane on the Ir(110)-(1×2) surface. In all cases the partial pressure of the hydrocarbon was 1.0 Torr. The optimal, statistically significant values of β are displayed in each case.

i.e. in the absence of a sufficient concentration of hydrogen adatoms, the reverse reaction of eq 3 will compete with the hydrogenation of the product fragments. If the product fragments are sufficiently hydrogen-deficient (i.e. two or more hydrogen atoms), the apparent order in P_{H_2} for the hydrogenation of the fragments will be unity or greater. Consequently, the mechanism described by eq 1–3 was altered to include also the case where the C–C bond cleavage reaction is reversible. We replace eq 3 with reaction 8 where $x = 2y$, and eq 5, the product fragment

$$C_nH_x(a) \rightleftarrows 2C_mH_y(a) \tag{8}$$

hydrogenation step, with the (set of) reaction(s)

$$C_mH_y(a) + 2\delta H(a) \rightarrow C_mH_{2m+2}(g) \tag{9}$$

where $y = 2(m - \delta) + 2$. An analysis, detailed elsewhere,[26] indicates that the "selectivity" of hydrogenation (i.e. the probability that the product fragments, once formed, will be hydrogenated) can be approximated by eq 10 where $k_h(T)$ is a combination of rate coefficients given explicitly elsewhere[26] and R_C is the rate of the C–C bond cleavage, which is given by eq 4. Utilizing that expression for R_C, the rate of hydrogenolysis becomes eq 11. Equation 11 predicts that the apparent order in P_{H_2} will vary from $\delta = (\alpha + 1)/2$ to zero and finally to $-(\alpha + {}^1/_2)$, as P_{H_2} is increased.

$$S_{hyd} \equiv R_{hyd}/R_C = k_hP_{H_2}{}^{\delta}/(1 + k_hP_{H_2}{}^{\delta}) \tag{10}$$

$$R_{hyd} = [k_CK^*P_{HC}/(K^*P_{HC} + P_{H_2}{}^{\alpha+1/2})][k_hP_{H_2}{}^{\delta}/(1 + k_hP_{H_2}{}^{\delta})] \tag{11}$$

The data for *n*-butane hydrogenolysis on the Ir(110)-(1×2) surface have been fit to eq 11. These results are shown in Figure 13c, where an optimal fit was obtained with $\alpha = 1$ and $\delta = 1$. Moreover, the quality of the fit (standard deviation 15%) is excellent. This result suggests that the major reaction channel for *n*-butane hydrogenolysis on Ir(110)-(1×2) involves reversible, symmetric C–C bond cleavage.

The data for the minor reaction channel for *n*-butane hydrogenolysis on Ir(110)-(1×2), i.e. $n\text{-}C_4H_{10} + H_2 \rightarrow CH_4 + C_3H_8$, can also be examined by employing either of the mechanistic schemes described above. These data are shown in Figure 14a in terms of the total $CH_4 + C_3H_8$ conversion and are described well by eq 4, the mechanism involving irreversible C–C bond cleavage, with either $\alpha = {}^1/_2$ or 1, the standard deviation being approximately 18% in both cases. Note that these parameters are essentially identical with those obtained for the major reaction channel on the Ir(111) surface.

The C_m selectivity in the rollover regime was examined quantitatively by employing eq 7. The results are shown in parts a and b of Figure 15 for propane and neopentane and in Figure 14b for the minor reaction channel of *n*-butane. In all cases, the standard deviation is less than approximately 10%. The stoichiometries of the product fragments implied by these data are given in Table VI. The stoichiometry of the product fragment for the major reaction channel of *n*-butane was determined previously by the agreement of the data with eq 11 for $\delta = 1$. Note that the product fragments from neopentane (and possibly propane) are the same on both the (111) and (110)-(1×2) surfaces (as was the case for the parent fragments).

IV. Discussion

A. Ethane. Ethane hydrogenolysis has been reported to be sensitive to changes in the average metallic particle size on silica-supported catalysts of both Rh[32,33] and Ni.[34] For example, Yates and Sinfelt[32] reported maximum specific activities on Rh/SiO_2 catalysts for average metal crystallite sizes between 10 and 40 Å, whereas, for particle sizes above 100 Å, the activity decreased by $1\text{–}1{}^1/_2$ orders of magnitude. Similar results were reported by Martin and Dalmon[34] on Ni/SiO_2 catalysts of varying particle size. Recent work by Lee and Schmidt[33] on Rh/SiO_2 catalysts and by Goodman[9] on oriented Ni single crystals suggests that the observed variations in the specific activity may be due to structural changes in the catalyst surface with increasing particle size. In particular, the work of Goodman[9] implicates the importance of the relative number of surface atoms in (100) and (111) microfacets of the metal crystallite as the particle size is varied.

In contrast to the observations on Rh and Ni, Foger and Anderson[22] reported differences in the specific activities on alumina- and silica-supported Ir of less than a factor of 3 between catalysts with average particle sizes of 15 and 70 Å. Apparently the nature of the metal exerts considerable influence on the degree of sensitivity of the catalytic properties to changes in the average particle size. However, it must be noted that comparisons based solely on specific activities at a particular set of reaction conditions can be misleading *unless* there happen to be no variations in the apparent reaction kinetics or apparent reaction orders in P_{HC} and P_{H_2}. Examination of the data obtained here with the (111) and (110)-(1×2) surfaces of Ir illustrates this point clearly; e.g., for temperatures below approximately 550 K, the (111) surface is more active than the (110)-(1×2), whereas, above 550 K, the opposite is true. This observation is a manifestation of the different apparent reaction kinetics observed on the two surfaces. For the limited temperature range examined by Foger and Anderson[22] ($T \cong 525$–550 K; cf. Figure 2), the specific activities on the Ir(111) and Ir(110)-(1×2) surfaces are very similar, supporting their observed lack of any strong sensitivity to particle size.

As may be seen from Tables II and V, the apparent reaction kinetics differ considerably for ethane hydrogenolysis (in the lower temperature linear Arrhenius regime) on the two surfaces considered here; i.e., $E_{app} \cong 35$ kcal·mol^{-1} and $k_{app}{}^{(0)} \cong 1 \times 10^{13}$ molecules·site^{-1}·s^{-1} on Ir(111) and $E_{app} \cong 49$ kcal·mol^{-1} and $k_{app}{}^{(0)} \cong 6 \times 10^{18}$ molecules·site^{-1}·s^{-1} on Ir(110)-(1×2). These differences can be explained by either different reaction mechanisms or the same mechanism in which the rates and energetics of one or more elementary steps differ. From Tables III and VI we see that distinct reaction intermediates are implicated on the two surfaces, namely, C_2H_4 on Ir(111) and C_2H_2 on Ir(110)-(1×2). Conse-

(32) Yates, D. J. C.; Sinfelt, J. H. *J. Catal.* **1967**, *8*, 348.
(33) Lee, C.; Schmidt, L. D. *J. Catal.* **1986**, *101*, 123.
(34) Martin, G. A.; Dalmon, J. A. *C. R. Seances Acad. Sci., Ser. C* **1978**, *286*, 127.

quently, the difference between the apparent reaction kinetics is evidently due to the different reaction intermediates. It is of interest to note that the correlation between a more extensively dehydrogenated intermediate and a higher apparent activation energy has been observed previously for ethane hydrogenolysis on a number of metals[35] and for the hydrogenolysis of various C_5 hydrocarbons on Pt/Al_2O_3 catalysts.[36] The most plausible explanation for this correlation involves the reaction mechanism described by eq 1–3. Specifically, the enthalpy change for the set of reactions $C_2H_6(g) + H(a) \rightarrow C_2H_x(a) + (\alpha + {}^1/_2)H_2(g)$[29] is considered to be positive (i.e. $\Delta H^\ddagger > 0$), and the endothermicity increases with greater values of α. Since $E_{app} \cong E_C + \Delta H^\ddagger$ for temperatures below the onset of rollover, the apparent activation energy will increase as α increases.

The difference between the apparent preexponential factors on two surfaces is also consistent with different reaction intermediates. As discussed in Section III.A, the apparent preexponential factor is expected to increase with an increasing extent of dehydrogenation of the adsorbed hydrocarbon fragment (i.e. increasing α). In particular, the mechanism of eq 4 predicts that an increase in the value of α from 1 to 2 will be accompanied by an increase in the apparent preexponential factor of approximately 3 orders of magnitude. This is in reasonable agreement with the observed difference of 5–6 orders of magnitude. Moreover, if one compares the ratio of the apparent preexponential factors for the low-temperature (where $k_{app}^{(0)} \cong k_C^{(0)}K^{\ddagger(0)}P_{HC}/P_{H_2}{}^{\alpha+1/2}$) and the high-temperature (where $k_{app}^{(0)} \cong k_C^{(0)}$) regimes, the observed difference between the two surfaces is approximately 3 orders of magnitude, in excellent agreement with the predicted result. It is of interest to note that this agreement between different values of α, which were determined at constant temperature and varying reactant partial pressures, and the different values for (the low-temperature) $k_{app}^{(0)}$, which were determined at constant reactant partial pressures and varying temperature, lends considerable support to the validity of the mechanism put forward here (eq 4).

The differing extents of dehydrogenation of the reaction intermediates on each surface can be explained by arguments based on structural considerations. It is generally accepted that ethane hydrogenolysis proceeds through an intermediate in which both carbon atoms are bound to the surface. The apparent reaction intermediate implicated on the Ir(111) surface, C_2H_4, is consistent with a species bound to the surface via two carbon–metal σ bonds. The apparent reaction intermediate implicated on the Ir(110)-(1×2) surface, C_2H_2, implies a higher degree of coordination (i.e. bond order) to the metal surface. In this connection, it should be recalled that the Ir(110)-(1×2) surface possesses high-coordination "trough" adsites (C_{11} atoms, cf. Figure 1[13]), which are not present on the Ir(111) surface. Consequently, it is quite conceivable that on the (110)-(1×2) surface a more extensively dehydrogenated hydrocarbon fragment may be formed, whereas, on the essentially flat (111) surface, its formation is not energetically favorable.

B. Propane. Compared to ethane, considerably less work has been carried out concerning propane hydrogenolysis by metal catalysts.[37-39] The first-row group VIII transition metals have been found to promote complete hydrogenolysis, i.e. the production of methane, with Ni exhibiting a somewhat higher selectivity for ethane compared to Fe and Co.[38] On the other hand, on both alumina-supported Ru[37,38] and Pt[39] and Pt blacks,[40] the selectivities for both ethane and methane have been found to be nearly equal; i.e., one carbon–carbon bond is cleaved. In all cases the apparent reaction orders with respect to P_{HC} were nearly unity, whereas those with respect to P_{H_2} were typically between −1 and −2, consistent with our observations here. Finally, the selectivity for ethane was found to decrease with increasing temperature.[37] This selectivity shift with increasing temperature is clearly associated with the rollover phenomena observed here.

Examination of the results given in Tables II and V shows that both the specific activities and the apparent kinetic parameters are essentially identical on the Ir(111) and Ir(110)-(1×2) surfaces. Furthermore, as may be seen from Tables III and VI, the stoichiometries of the adsorbed parent hydrocarbon fragments are also identical. These observations suggest strongly that the reaction mechanism on both surfaces is the same.

Knowledge of the stoichiometries of the adsorbed intermediates, coupled with comparisons to the other reactions considered here, permits speculation as to the nature of the dominant mechanism. For example, the stoichiometry of the adsorbed intermediate, C_3H_6, is consistent with a species bound to the surface via two single carbon–metal bonds, which may involve more than one metal surface atom. Since different adsorbed intermediates were implicated for ethane on the two surfaces and ethane must be bound 1,2, it is probable that this species is bound through the terminal carbon atoms, i.e. 1,3 adsorption. A 1,3 diadsorbed species is consistent with either a mononuclear metallacycle butane[41] or a binuclear metallacycle pentane.[42] Interconversion between metallacycle butanes and metallacarbenes and adsorbed olefins is well-known in organometallic chemistry and is of special importance to olefin metathesis.[43] Not surprisingly, the importance of metallacycle butanes in heterogeneous catalysis and the hydrogenolysis of alkanes has been suggested previously.[5] Carbon–carbon bond cleavage of a metallacycle butane to form a methylidene and adsorbed ethylene, followed by rapid hydrogenation of these species, would be consistent with our experimental observations, i.e. production of methane and ethane. On the other hand, a binuclear metallacycle pentane also provides an attractive candidate for the reaction intermediate. For example, for an sp^3-hybridized $C_3H_6(a)$ species, the C_1–C_3 internuclear distance is approximately 2.52 Å, a value which is within 10% of the nearest-neighbor Ir–Ir spacing of 2.72 Å. Consequently, we would expect minimal C–C bond strain in the carbon framework for a binuclear metallacycle pentane. Obviously, it is impossible to discriminate between these proposals on the basis of our results.

We have also measured the specific rates of hydrogenolysis of cyclopropane on both the Ir(111) and Ir(110)-(1×2) surfaces.[18] These data can be used to lend considerable support to our interpretation of the rollover phenomenon via the use of eq 4. The reaction of cyclopropane with hydrogen on these two Ir surfaces was found to follow two distinct reaction pathways; the major product was propane, whereas the minor products were equal amounts of ethane and methane.[18] Since variation of the reactant partial pressures indicated that the reaction rate via the minor channel $c\text{-}C_3H_6 + 2H_2 \rightarrow CH_4 + C_2H_6$ was essentially zero order in both P_{HC} and P_{H_2}, the apparent kinetics of this minor reaction channel was not affected by a pseudoequilibrium between the gas-phase reactants and an adsorbed hydrocarbon fragment (i.e. the dissociative adsorption of cyclopropane is irreversible). Rather, the hydrogenolysis of cyclopropane to methane and ethane is limited by the decomposition (C–C bond cleavage) of an adsorbed hydrocarbon species that is formed readily from cyclopropane compared to propane, e.g. ring opening of cyclopropane to form a diadsorbed species, $C_3H_6(a)$. Thus, for cyclopropane, the apparent reaction kinetics should reflect directly the energetics of the (secondary for cyclopropane) C–C bond cleavage reaction.

The specific rates of hydrogenolysis (to ethane and methane) of both propane and cyclopropane on the Ir(110)-(1×2) surface are shown in Figure 16 in terms of conversion. There is an *excellent* correlation between the apparent activation energy of

(35) Sinfelt, J. H.; Taylor, W. F.; Yates, D. J. C. *J. Phys. Chem.* **1965**, *69*, 95.
(36) Garin, F.; Gault, F. G. *J. Am. Chem. Soc.* **1975**, *97*, 4466.
(37) Machiels, C. J.; Anderson, R. B. *J. Catal.* **1979**, *58*, 253.
(38) Tajbl, D. G. *Ind. Eng. Chem. Prod. Res. Dev.* **1969**, *8*, 364.
(39) Leclercq, G.; Leclercq, L.; Maurel, R. *J. Catal.* **1976**, *44*, 68.
(40) Guczi, L.; Sarkany, A.; Tetenyi, P. *J. Chem. Soc., Faraday Trans. 1* **1974**, *70*, 1971.
(41) Herrison, J. L.; Chauvin, Y. *Makromol. Chem.* **1970**, *141*, 161.
(42) See, e.g.: Theopold, K. H.; Bergman, R. G. *J. Am. Chem. Soc.* **1980**, *102*, 5695. Motyl, K. M.; Norton, J. R.; Schauer, C. K.; Anderson, O. P. *J. Am. Chem. Soc.* **1982**, *104*, 7325. Krause, M. J.; Bergman, R. G. *J. Am. Chem. Soc.* **1985**, *107*, 2972.
(43) Grubbs, R. H. *Prog. Inorg. Chem.* **1978**, *24*, 1. Calderon, N.; Lawrence, J. P.; Ofstead, E. A. *Adv. Organomet. Chem.* **1979**, *17*, 449.

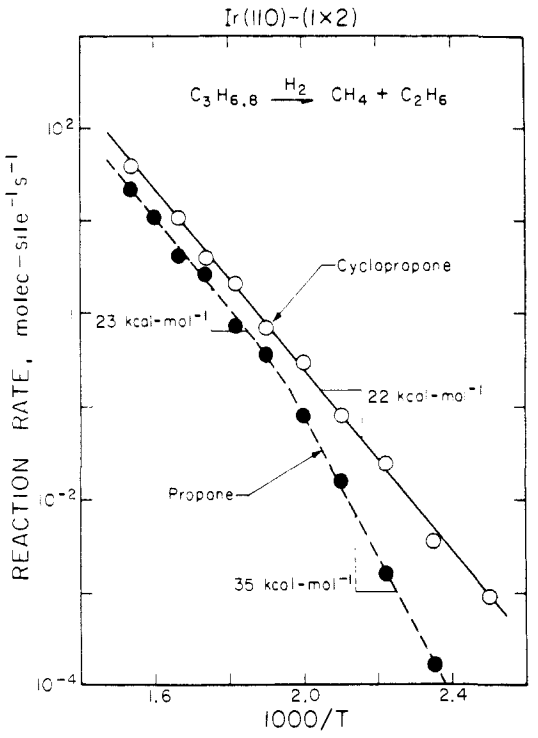

Figure 16. Specific rates of hydrogenolysis of propane (this work) and cyclopropane[18] to ethane and methane on the Ir(110)-(1×2) surface. The partial pressure of propane was 1.0 Torr, that of cyclopropane was 2.0 Torr, and that of hydrogen was 100 Torr. The values displayed for the apparent activation energies were obtained from least-squares fits to the total rate of conversion to methane and ethane.

propane hydrogenolysis for temperatures above the onset of rollover and that of cyclopropane hydrogenolysis. (Note also that rollover, with respect to changes in the apparent activation energy, does not occur for cyclopropane under these reaction conditions.) In addition, for $T \geq 525$ K, the specific rates of reaction are within a factor of 2. This correlation supports our assignment of the apparent activation energy below rollover to the quantity $E_C + \Delta H^{\ddagger}$, where $\Delta H^{\ddagger}$ is positive, and that above, solely to the activation energy of the C–C bond cleavage reaction, E_C. Specifically, the enthalpy change for $C_3H_8(g) + H(a) \rightarrow C_3H_6(a) + {}^3/_2H_2(g)$ implicated by these data is approximately 12–13 kcal·mol^{-1}.

This value for $\Delta H^{\ddagger}$ can be used to calculate the "binding energy" of the adsorbed hydrocarbon fragment, $C_3H_6(a)$. (More specifically, this calculation should approximate well the energy difference between the adsorbed fragment $C_3H_6(a)$, assumed to be bound 1,3, and the biradical $^{\bullet}CH_2CH_2CH_2^{\bullet}(g)$.) In particular, $\Delta H^{\ddagger} = 2D_{C-H} - {}^1/_2\Delta H_{H_2} - D_{H-H} - D_{Ir=C_3H_6}$, where D_{C-H} (D_{H-H}) is the C–H (H–H) bond dissociation energy (D_{C-H}, more rigorously, is the average value for the two reactions $C_3H_8 \rightarrow CH_3CH_2CH_2^{\bullet} + H^{\bullet}$ and $CH_3CH_2CH_2^{\bullet} \rightarrow {}^{\bullet}CH_2CH_2CH_2^{\bullet} + H^{\bullet}$), ΔH_{H_2} is the heat of adsorption of hydrogen on Ir(110)-(1×2), and $D_{Ir=C_3H_6}$ is the binding energy of the reaction intermediate. Assuming propane adsorbs 1,3, then $D_{C-H} \cong 98$ kcal·mol^{-1}, whereas for the expected high coverages of hydrogen adatoms under our reaction conditions, $-\Delta H_{H_2} \leq 10$ kcal·mol^{-1}.[19] Utilizing these values and $D_{H-H} \cong 104$ kcal·mol^{-1}, we find that $D_{Ir=C_3H_6} \cong 85 \pm 1$ kcal·mol^{-1}, which implies a single-order carbon–iridium bond strength of 42–43 kcal·mol^{-1}.

C. *n*-Butane. The study of the hydrogenolysis of *n*-butane permits an examination of selectivity, in addition to activity, variations with surface structure, since for a reaction involving the cleavage of a single C–C bond, two product distributions are possible, i.e. $CH_4 + C_3H_8$ and $2C_2H_6$. As was the case with propane, "complete" hydrogenolysis to methane has been found to predominate on Ni,[10,44] whereas the three expected products

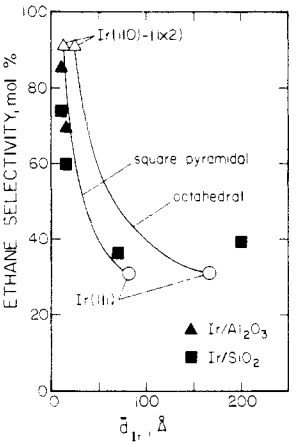

Figure 17. Selectivity for ethane production (mol % of total products) from the reaction of *n*-butane with hydrogen on Ir catalysts plotted as a function of the mean Ir particle size. Data for the supported catalysts are from Foger and Anderson.[22] The abscissae for the two single crystalline surfaces were determined by a calculated "effective particle size", as described in the text. The solid curves represent theoretical interpolations between the single crystalline surfaces based on the specified geometrical shapes, as described in the text. The reaction temperature in all cases is approximately 475 K.

(CH_4, C_2H_6, and C_3H_8) were formed in approximately equal amounts on alumina-supported Ru.[45] Of particular interest here, over both Pt-[46] and Ir-supported[22] catalysts, the product distributions have been found to be sensitive to the metal particle size; in particular, the selectivity for ethane production was found to increase dramatically as the particle size decreased.[47]

Foger and Anderson[22] have reported that the selectivity for the hydrogenolysis of *n*-butane is extremely sensitive to the average metallic particle size. This structure sensitivity is most evident for clusters of diameter ≤40 Å, where there is a rapid change in the average coordination number of the metal surface atoms.[13,48] The immediate implication of these results is that the mechanism and, hence, the catalytic selectivity are dictated by the structure of the surface. In order to quantify the connection between the catalytic selectivity and the local surface structure, we have compared these results for supported Ir catalysts of varying particle size to those obtained here on the Ir(111) and Ir(110)-(1×2) surfaces.[49]

In order to make this comparison, we have computed an "effective particle size"[49] for the (111) and (110)-(1×2) surfaces, utilizing the ratio of the number of edge (C_7) atoms to the number of (111) face (C_9) atoms as the appropriate criterion.[50] For example, the (110)-(1×2) surface contains one C_7 atom and two C_9 atoms per unit cell, a ratio of 1/2. The ratio for the (111) surface is determined by both defects and the edge of the crystal (edge area/surface area ≤ 1/10). For a perfect (111) surface it would be zero. On the basis of hydrogen chemisorption data,

(44) Anderson, J. R.; Baker, B. G. *Proc. R. Soc. London, A* **1963**, *402*, A271.

(45) Kempling, J. C.; Anderson, R. B. *Ind. Eng. Chem. Prod. Res. Dev.* **1970**, *9*, 116.

(46) (a) Leclercq, G.; Trochet, J.; Maurel, R. *C. R. Seances Acad. Sci., Ser. C* **1973**, *276*, 1353. (b) Guczi, L.; Gudkov, B. S. *React. Kinet. Catal. Lett.* **1978**, *9*, 343.

(47) A high selectivity for ethane production from the hydrogenolysis of *n*-butane has been observed also for Pt-Ir/Al_2O_3 bimetallic catalysts, see: Bernard, J. R.; Bousquet, J.; Turlier, P. *Proc. Int. Congr. Catal., 7th* **1980**, paper A7.

(48) Poltorak, O. M.; Boronin, V. S. *Russ. J. Phys. Chem. (Engl. Transl.)* **1966**, *40*, 1436.

(49) Engstrom, J. R.; Goodman, D. W.; Weinberg, W. H. *J. Am. Chem. Soc.* **1986**, *108*, 4653.

(50) Alternatively, we could have computed the C_7/C_9 ratio of the supported metal particles and evaluated the ethane selectivity as a function of this ratio.[48] However, this calculation presumes that both the particle shape and the effective diameters of the supported catalysts are known to high accuracy. Since we do know the C_7/C_9 ratio to high accuracy for the single crystals, we have chosen to compute "effective particle diameters".

(51) See, e.g.: Brunelle, J.-P.; Sugier, A.; Le Page, J.-F. *J. Catal.* **1976**, *43*, 273.

which have been shown to be sensitive to the presence of defects such as atomic steps,[19] the ratio for this (111) surface is approximately 1/20. Assuming the supported catalyst particles form shapes of either octahedral or square-pyramidal (half-octahedral) structure,[52] we find that the effective mean particle diameters are approximately 24 or 13 Å for the Ir(110)-(1×2) surface and 166 or 81 Å for the (111) surface, respectively.[53]

The selectivity for ethane production for both the supported catalysts[22] and the two single crystalline surfaces is shown in Figure 17 as a function of the mean particle diameter.[54] Theoretically calculated curves, normalized to the specific activities of the two single crystalline surfaces and interpolated by using the ratio C_7/C_9 as a basis, are also shown in Figure 17. Obviously, there is an excellent correlation between the selectivity for ethane production and the mean Ir particle size. On the basis of our results, the observed increase in ethane selectivity with decreasing particle size is identified clearly with the increasing participation of low coordination number surface atoms.

The observed correlation between the Ir(110)-(1×2) surface examined here, i.e. a massive single crystal, and the supported Ir crystallites of 10–15-Å mean diameter examined by Foger and Anderson[22] suggests that there is little difference between the electronic properties of the low coordination surface atoms present on each. This is entirely reasonable. For example, Ir crystallites of 10–15-Å mean diameter correspond to clusters containing approximately 50–150 atoms. UV photoelectron spectroscopic measurements on Pt clusters as a function of particle size by Baetzold[55] indicate that as few as 25 atoms are sufficient to produce surface electronic properties typical of much larger crystals, such as those examined here. Likewise, photoionization spectra of Fe clusters obtained by Cox et al.[56] indicate that the ionization potential approaches that of the bulk metal for clusters containing 25 atoms. Thus, we conclude that the correlation observed here is due to the local coordination of the surface atoms and not, for example, due to some fortuitous agreement caused by an intrinsic variation in electronic properties with the size of the supported Ir crystallites.[52]

Examination of the results given in Tables II and V for the apparent reaction kinetics and in Tables III and VI for the implied stoichiometries of the reaction intermediates suggests strongly that different mechanisms are operative for *n*-butane hydrogenolysis on the Ir(111) and Ir(110)-(1×2) surfaces. For example, on the Ir(111) surface both the activity and apparent reaction kinetics for the hydrogenolysis of propane and *n*-butane are very similar to one another, implicating similar reaction pathways. However, for *n*-butane hydrogenolysis on the Ir(110)-(1×2) surface, the apparent reaction kinetics, the implied reaction intermediates, and the selectivity all differ considerably from those observed on the Ir(111) surface for *n*-butane and on both surfaces for propane. These observations virtually assure that a distinct reaction mechanism is operative on the (110)-(1×2) surface for *n*-butane hydrogenolysis. As demonstrated in Figure 13c, the mechanism providing the best fit to the data is given by

$$n\text{-}C_4H_{10}(g) \rightleftarrows C_4H_8(a) + 2H(a)$$

$$C_4H_8(a) \rightleftarrows 2C_2H_4(a)$$

$$C_2H_4(a) + 2H(a) \rightarrow C_2H_6(g)$$

The stoichiometry of the parent fragment, C_4H_8, is consistent with a di-σ-bonded intermediate. However, in this case, the most plausible structure is a 1,4 diadsorbed species or, more specifically, a metallacycle pentane. The importance of 1,4 intermediates in alkane hydrogenolysis has been suggested by both Leclercq et al.[57] and Zimmer et al.,[58] on the basis of the observation that 2,2,3,3-tetramethylbutane cleaves readily to isobutane on Pt/Al_2O_3 and Pt blacks, and by Kane and Clarke,[59] on the basis of the observation of a high selectivity for the production of ethane and isobutane from the hydrogenolysis of 2,2-dimethylbutane on Pt–Au films.[60] However, the most compelling evidence derives from precedents in organometallic chemistry, for example, the work of Grubbs and co-workers,[62] concerning reversible bis(olefin)–metallacycle pentane interconversion in homogeneous transition-metal complexes. It is known that transition-metal complexes containing metallacycle pentane ligands can decompose thermally to two ethylene ligands,[62] i.e. the exact reaction implicated by the mechanism shown above.

Further evidence for the metallacycle intermediate (implicitly mononuclear) can be provided if one considers its stereochemistry on the two Ir surfaces. For example, utilizing bond lengths and bond angles for Ir[63] and Pt[64] complexes containing metallacycle pentane ligands, one finds that significant repulsion is expected between the α-hydrogens and the adjacent Ir atoms on a (111) surface. However, no such repulsion is expected if one coordinates the ligand about the low coordination number C_7 atom on the (110)-(1×2) surface. Since these C_7 atoms are not present on the (111) surface, the absence of the mononuclear metallacycle pentane intermediate on Ir(111) can be explained purely on a stereochemical basis.

Anderson and co-workers[65] have suggested previously that the formation of "carbocyclic" intermediates, which were suggested to be partially responsible for the skeletal isomerization of C_5 and C_6 hydrocarbons on Pt (especially for highly dispersed catalysts), is favored on low coordination number surface metal atoms. Although this interpretation has been questioned,[5] a complete understanding is hampered by the fact that there are apparently two "cyclic" mechanisms, "selective" and "nonselective".[66] Finlayson et al.[67] have demonstrated recently that the selective mechanism for the cyclization of 2,2,4,4-tetramethylpentane on Ir, Pt, Rh, and Pd films proceeds through a 1,5 di-σ-bonded intermediate, presumably a mononuclear metallacycle hexane. Since the C–Ir–C bond angle is certainly greater for a metallacycle hexane compared to a metallacycle pentane, we would predict that this "selective cyclic mechanism" is sterically forbidden on the Ir(111) surface. This conclusion extends the proposition of

(52) See, e.g.: Burch, R. In *Catalysis (Specialist Periodical Reports)*; Bond, G. C., Webb, G., Eds.; Royal Society of Chemistry: London, **1985**, Vol. 8, p 149, and references therein.

(53) These two geometrical shapes bracket other probable regular polyhedra, e.g. cubooctahedra or cubes.

(54) Note that, for the reaction $n\text{-}C_4H_{10} + H_2 \rightarrow 2C_2H_6$, the selectivity for ethane is 100%, whereas, for the reaction $n\text{-}C_4H_{10} + 2H_2 \rightarrow 2CH_4 + C_2H_6$, the selectivity for ethane is 33%.

(55) Baetzold, R. C. *Inorg. Chem.* **1982**, *21*, 2189.

(56) Rohlfing, E. A.; Cox, D. M.; Kaldor, A.; Johnson, K. H. *J. Chem. Phys.* **1984**, *81*, 3846.

(57) Leclercq, G.; Leclercq, L.; Maurel, R. *J. Catal.* **1977**, *50*, 87.

(58) Zimmer, H.; Tetenyi, P.; Paal, Z. *J. Chem. Soc., Faraday Trans. 1* **1982**, *78*, 3573.

(59) Kane, A. F.; Clarke, J. K. A. *J. Chem. Soc., Faraday Trans. 1* **1980**, *76*, 1640.

(60) It is of interest to note that Zimmer et al.,[58] examining the rates of C–C bond cleavage (hydrogenolysis) of substituted butanes at the C_2–C_3 bond, observed maxima in the specific rates with respect to P_{H_2} consistent with our observations for *n*-butane on Ir(110)-(1×2). On the basis of our mechanism involving metallacycle pentane–bis(olefin) interconversion, the specific value of P_{H_2} at the maximum should be inversely proportional to the rate of hydrogenation of the resulting olefins. Since the rate of olefin hydrogenation decreases with increasing alkyl substitution about the double bond,[61] i.e. the rates of hydrogenation follow the order ethylene > propylene > isobutylene, we would expect that the maxima in P_{H_2} for the hydrogenolysis of substituted butanes will follow the order 2,2-dimethylbutane < 2,2,3-trimethylbutane < 2,2,3,3-tetramethylbutane. Indeed, this is exactly what Zimmer et al. observed.[58]

(61) Kraus, M. *Adv. Catal.* **1980**, *29*, 151.

(62) Grubbs, R. H.; Miyashita, A. *J. Am. Chem. Soc.* **1978**, *100*, 1300. Grubbs, R. H.; Miyashita, A.; Liu, M.; Burk, P. *J. Am. Chem. Soc.* **1978**, *100*, 2418.

(63) (a) Fraser, A. R.; Bird, P. H.; Bezman, S. A.; Shapley, J. R.; White, R.; Osborn, J. A. *J. Am. Chem. Soc.* **1973**, *95*, 597. (b) Diversi, P.; Ingrosso, G.; Lucheni, A.; Porzio, W.; Zocchi, M. *J. Chem. Soc., Chem. Commun.* **1977**, 811.

(64) Cheethan, A.; Puddephatt, R. J.; Zalkin, A.; Templeton, D. H.; Templeton, L. K. *Inorg. Chem.* **1976**, *15*, 299.

(65) Anderson, J. R.; MacDonald, R. J.; Shimoyama, Y. *J. Catal.* **1971**, *20*, 147.

(66) Maire, G.; Plouidy, G.; Prudhomme, J. C.; Gault, F. G. *J. Catal.* **1965**, *4*, 556.

(67) Finlayson, O. E.; Clarke, J. K. A.; Rooney, J. J. *J. Chem. Soc., Faraday Trans. 1* **1984**, *80*, 191.

Finlayson et al.[67] that substitution at the 1,5 terminal carbon atoms (e.g. alkyl groups) will sterically hinder metallacycle hexane formation, i.e. the α-hydrogens should provide sufficient steric hindrance on the (111) surface.

Finally, the apparent reversibility of metallacycle pentane and bis(ethylene) interconversion observed here on the Ir(110)-(1×2) surface (the reversibility consistent with the work of Grubbs et al.[62]) suggests that this mechanism may be important for the isomerization of higher hydrocarbons, e.g. branched butanes or pentanes. For example, Garin et al.[68] have invoked 1,2 and 1,3 ethyl-shift mechanisms to explain the product distribution from the isomerization of ^{13}C-labeled 2- and 3-methylpentanes on alumina-supported Ir catalysts. Interestingly, these mechanisms predominated on the most highly dispersed catalysts studied ($\bar{d}_{Ir} \cong 10$ Å). We note that virtually all of their experimental observations can be rationalized by invoking a mechanism involving reversible metallacycle (substituted) pentane–bis(olefin) interconversion. For example, for 3-methylpentane the olefins would be ethylene and 1-butene. If one permits rotation about and/or migration of the double bond(s) prior to recyclization, the former of which has been observed experimentally for homogeneous complexes,[62] the isomerization product distribution can be accounted for completely. The fact that these mechanisms predominate on highly dispersed catalysts that contain a large fraction of low coordination number surface metal atoms lends further support to our proposition.

D. Neopentane. The reaction of neopentane with hydrogen on transition-metal catalysts, especially on Pt,[69] has attracted particular interest since both isomerization (to isopentane) and hydrogenolysis products have been observed. In addition, correlations have been made between the fraction of surface atoms in (111) microfacets and the isomerization selectivity with respect to that of hydrogenolysis.[69-71] Specifically, isomerization is favored on large metal crystallites of low dispersion. However, as discussed in section III.A, there is considerable disagreement concerning the observation of the isomerization of neopentane on iridium catalysts.[21-24] In cases where isomerization was observed,[21,22] its specific rate was less than $^1/_3$ that of hydrogenolysis. Finally, if the concentration of (111) microfacets influences the mechanism of the reaction of neopentane on Ir, a comparison of the (111) and (110)-(1×2) surfaces will be of little use, since, in terms of C_9 atoms or 3-fold hollow (B_3) sites,[13] the densities of these microfacets are nearly equal (and nearly equally accessible to a neopentane molecule) on the two single crystalline surfaces.

An examination of Tables II, III, V, and VI shows that the specific activities, the apparent reaction kinetics, and the implied reaction intermediates (both parent and product) are essentially identical on the Ir(111) and Ir(110)-(1×2) surfaces. As with propane, these observations implicate the presence of similar reaction mechanisms on these two surfaces. However, unlike propane, the parent hydrocarbon fragment from neopentane is extensively dehydrogenated; i.e., apparently four or five hydrogen atoms are removed. This extent of dehydrogenation suggests that three carbon atoms may be bound to the surface, à la the "triadsorbed" intermediate proposed previously by Anderson and Avery,[25] although 1,3 diadsorption cannot be excluded.

Isomerization products of neopentane were not detected on either surface. Nevertheless, the formation of ethane and propane may follow a similar reaction channel. That is, if ethane and propane merely resulted from successive "demethylizations" of the parent neopentane molecule, we would not expect ethane and propane to be formed in equal amounts (i.e. stoichiometrically). On the other hand, if neopentane were to isomerize to an adsorbed (dehydrogenated) isopentane species, a single C–C bond cleavage in this intermediate could result in the production of equal amounts of ethane and propane. As may be seen in Figure 2d, ethane and propane are not produced stoichiometrically at any reaction temperature on the Ir(111) surface. However, as shown in Figure 5, these two products behave similarly with respect to P_{HC} and P_{H_2}. On Ir(110)-(1×2), as shown in Figure 9d, ethane and propane are produced stoichiometrically at a temperature of 475 K, and the products behave similarly with respect to P_{HC} and P_{H_2}, as shown in Figure 12. These observations suggest that ethane and propane may be formed from a isopentane "precursor" on the (110)-(1×2) surface, since single C–C bond cleavage of isopentane can produce ethane and propane (stoichiometrically). Moreover, central C–C bond cleavage of 2-methylbutane (i.e. isopentane) on the Ir(110)-(1×2) surface is consistent with the observed dominant formation of ethane from *n*-butane on this surface.

V. Conclusions

We have examined the hydrogenolysis of various short-chain alkanes on the Ir(111) and Ir(110)-(1×2) surfaces in order to quantify the relationship between surface structure and both catalytic activity and selectivity. These two surfaces were chosen in order to evaluate the role of low coordination number metal surface atoms in alkane hydrogenolysis. We have employed four different hydrocarbons of differing size and structure in an attempt to isolate and investigate the importance of a number of possible adsorption mechanisms. These mechanisms, or, equivalently, the adsorbed reaction intermediates, act to control the catalytic selectivity.

Postreaction surface analysis revealed the presence of a carbonaceous residue, the coverage of which was always at submonolayer levels, essentially independent of reaction conditions, i.e. surface temperature and reactant partial pressures. The coverage of the carbonaceous residue was nearly identical on both surfaces, and it increased approximately linearly with the number of carbon atoms in the parent hydrocarbon. Titration of these residues with hydrogen produced only methane, demonstrating that the carbonaceous residue essentially plays the role of a "spectator"; i.e., it is not a participant in the major reaction channels.

The major reaction channels for all of the reactants examined, with the exception of *n*-butane on the Ir(111) surface, involved the cleavage of a single carbon–carbon bond. These major reaction channels could be described by a demethylization of the parent hydrocarbon, with the exception of *n*-butane on the Ir(110)-(1×2) surface, which produced two ethane molecules. In all cases, as the temperature was increased sufficiently, the apparent activation energy decreased, and, concomitantly, the relative production of methane increased greatly. These changes, which we have designated as rollover, are associated with a depletion in the steady-state concentration of hydrogen adatoms. This was demonstrated explicitly by varying the hydrogen partial pressure at a temperature near the onset of rollover. Furthermore, since rollover occurred at a higher temperature on the Ir(110)-(1×2) surface, which contains hydrogen adsites characterized by a higher binding energy with respect to the (111) (in the limit of both low and high coverages),[19] we were able to identify the source of the hydrogen with the metal surface and not the carbonaceous residue.

A mechanistic model involving a rate-limiting, irreversible, unimolecular C–C bond cleavage step,[26] similar to those proposed previously by both Cimino et al.[15] and Sinfelt,[16] was able to describe the variations in the specific rates of hydrogenolysis with variations in both the temperature and the reactant partial pressures. In order to describe both the specific activity and the selectivity of hydrogenolysis, it was noted that the mechanism could be tested most sensitively by varying the reaction conditions at a temperature near the onset of rollover. The apparent kinetic parameters were found to be consistent with theoretical expectations on the basis of assumed, physically reasonable preexponential factors for each of the elementary surface reactions involved.[26] The successful application of the mechanism permitted the deduction of the stoichiometries of the adsorbed parent hydrocarbon fragments (i.e. the reaction intermediates). In all cases, the implied stoichiometries were consistent with the proposition that hydrogenolysis proceeds through a partially dehydrogenated intermediate that is multiply bound to the surface via one or more metal surface atoms. Examination of the variation in the selectivity

(68) Garin, F.; Girard, P.; Weisang, F.; Maire, G. *J. Catal.* **1981**, *70*, 215.
(69) Boudart, M.; Aldag, A. W.; Ptak, L. D.; Benson, J. E. *J. Catal.* **1968**, *11*, 35.
(70) Foger, K.; Anderson, J. R. *J. Catal.* **1978**, *54*, 318.
(71) Dominguez, J. M.; Yacaman, M. J. *J. Catal.* **1980**, *64*, 223.

as the hydrogen pressure was varied in the rollover regime also permitted the deduction of the stoichiometries of the adsorbed product hydrocarbon fragments. The hydrogenolysis of *n*-butane on the Ir(110)-(1×2) surface could not be described by the mechanism involving irreversible C–C bond cleavage. Rather, a mechanism involving reversible C–C bond cleavage in a symmetrical reaction intermediate was found to provide a superior fit to the data.

Ethane hydrogenolysis was determined to proceed through different reaction intermediates, the parent fragment on the Ir-(110)-(1×2) surface being more extensively dehydrogenated. We interpreted this result as a manifestation of the availability of high-coordination adsites on the (110)-(1×2) surface. Both propane and neopentane hydrogenolysis were found to be nearly indistinguishable on the two surfaces. These results can be interpreted by invoking reaction intermediates that are bound to two or more adjacent metal surface atoms. However, the participation of a mononuclear metallacycle butane in the hydrogenolysis of propane remains a distinct possibility. Comparing the specific rates of hydrogenolysis (to methane and ethane) of propane and cyclopropane[18] on the Ir(110)-(1×2) surface, we have lent considerable support to our assignment of the apparent activation energy to $E_{app} \cong E_C + \Delta H^*$ for temperatures below rollover and $E_{app} \cong E_C$ for temperatures above rollover.

The selectivity for the hydrogenolysis of *n*-butane on the two surfaces has been identified with the occurrence of particular, adsorbed reaction intermediates on each surface. When our results are compared to those reported previously on supported iridium catalysts of varying metallic particle size,[22] a direct correlation has been discovered between the selectivity for ethane production and the concentration of low coordination number metal surface atoms.[49] On the basis of the implicated reaction mechanism and precedents from organometallic chemistry,[62] the adsorbed reaction intermediate that leads to the high selectivity for ethane is a mononuclear metallacycle pentane, the formation of which is sterically forbidden on the (111) surface. The logical extension of this observation has led us to propose that other mechanisms involving, for example, mononuclear metallacycle hexanes[67] may also be forbidden on (111) surfaces. On the other hand, the observed reversibility of the metallacycle pentane–bis(ethylene) interconversion has led us to propose that these metallacycle pentane intermediates may be involved in the isomerization of higher hydrocarbons such as branched butanes and pentanes, particularly on highly dispersed catalysts.

Acknowledgment. This work was performed at Sandia National Laboratories and supported by the U.S. Department of Energy under Contract DE-AC04-76DP00789. We acknowledge the partial support of the Office of Basic Energy Sciences, Division of Chemical Science (D.W.G.), and National Science Foundation Grant No. DMR-8500789 (W.H.W.).

Registry No. C_2H_6, 74-84-0; C_3H_8, 74-98-6; C_4H_{10}, 106-97-8; *neo*-C_5H_{12}, 463-82-1; Ir, 7439-88-5.

Supplementary Material Available: Details of mechanistic modeling of the hydrogenolysis of alkanes on iridium and the microscopic significance of kinetic parameters (11 pages). Ordering information is given on any current masthead page.

Matrix Isolation Infrared Studies of Nucleic Acid Constituents. 5.† Experimental Matrix-Isolation and Theoretical ab Initio SCF Molecular Orbital Studies of the Infrared Spectra of Cytosine Monomers

M. Szczesniak,‡ K. Szczepaniak, J. S. Kwiatkowski,§ K. KuBulat, and W. B. Person*

Contribution from the Department of Chemistry, University of Florida, Gainesville, Florida 32611. *Received March 21, 1988*

Abstract: Results are presented from an experimental study of the infrared spectra of cytosine and its deuteriated derivatives isolated in an inert Ar matrix and also in an N_2 matrix deposited on a window at 15 K. These spectra show that isolated cytosine exists under these conditions as a mixture of the "normal" amino–oxo (a–o) tautomer and the "rare" amino–hydroxy (a–h) tautomer; in fact, the last form predominates in both matrices with an "equilibrium constant" $K_t(o/h) = [a–o]/[a–h]$ measured to be about 0.5. Infrared spectra of the crystalline solid are also presented, and they agree with the conclusion from X-ray diffraction studies that only the normal amino–oxo tautomer occurs in the solid. In order to interpret the observed infrared spectra, we have carried out an ab initio molecular orbital calculation of the spectra of both tautomers at the SCF level with a 3-21G basis set. The calculation predicts frequencies, absolute infrared intensities, and potential energy distributions (PEDs) for all normal modes of each tautomer to provide a basis for the assignment of the experimental spectra. The latter problem was aided greatly by the discovery that irradiation of cytosine isolated in an Ar matrix with UV light changes the relative concentrations of the two tautomers in the matrix. Application of this technique in our studies allowed us to separate the absorption spectra to obtain the complete infrared spectrum for each tautomer free from the absorption by the other form. Each separate spectrum was thus assigned with a reasonable degree of confidence by comparison with the calculated spectra. The relatively good agreement between calculated and experimental spectra for each tautomer provides support for confidence in the validity of the use of these calculated vibrational parameters as a basis for predicting spectra of cytosine and its derivatives. Finally, the effect of intermolecular interaction upon the spectrum of cytosine is examined in a comparison of the spectra of matrix-isolated samples with the spectrum of the crystalline solid.

Vibrational spectra of cytosine and of its corresponding nucleoside and nucleotide, as well as of several of its derivatives, have been the subject of numerous experimental studies in solution and in the solid phase (ref 1 and references given therein). These studies establish the predominance of the amino–oxo form for the cytosine residue, which is the same form as is considered to be involved in the base-pairing scheme in DNA.

Although studies of the vibrational spectra of nucleic acid bases such as cytosine in the solid state or dissolved in polar solutions

† Part 4 of this series is ref 23.

‡ On leave (1986–1988) from the Institute of Physics, Polish Academy of Sciences, 02-668 Warsaw, Poland.

§ On leave (1985–1986) from the Institute of Physics, N. Copernicus University, 87-100 Torun, Poland.

(1) Kwiatkowski, J. S.; Pullman, B. *Adv. Heterocycl. Chem.* **1975**, *18*, 199.

0002-7863/88/1510-8319$01.50/0